



DEPARTMENT OF INFORMATICS

TECHNISCHE UNIVERSITÄT MÜNCHEN

Master's Thesis in Robotics, Cognition, Intelligence

Comparison of Controllers for Trunk Stabilization in a Bipedal Robot

Felix Schausberger





DEPARTMENT OF INFORMATICS

TECHNISCHE UNIVERSITÄT MÜNCHEN

Master's Thesis in Robotics, Cognition, Intelligence

Comparison of Controllers for Trunk Stabilization in a Bipedal Robot

Vergleich von Reglern für die Rumpfstabilisierung in einem zweibeinigen Roboter

Author:	Felix Schausberger
Supervisor:	Dr.-Ing. Daniel Renjewski
Advisor:	Dr.-Ing. Daniel Renjewski
Submission Date:	15.03.2023



I confirm that this master's thesis in robotics, cognition, intelligence is my own work and I have documented all sources and material used.

Munich, 15.03.2023

Felix Schausberger

Acknowledgments

Firstly I would like to thank my advisor Dr.-Ing. Daniel Renjewski for his dedicated involvement and support through the past few months. He made this thesis possible in the first place. Furthermore, I want to thank Julian Schausberger as the second reader of this thesis for his open ears and insightful comments. I would also like to offer my gratitude to my friend, Lilla Nagy, who I collaborated with through the years while at Technical University of Munich (TUM). Thank you for always being dependable and I wish you all the best in your academic pursuits. A big thank you to Melina Neuß for always being available to supply me with the parts and the laughs needed to get through this project. Lastly but most importantly, I am eternally grateful to my parents, Klaus and Brigitta Schausberger, who have always given me a free hand in my career decisions and supported me in everything I have done. Thank you.

Abstract

Balancing the trunk on long legs is a major challenge in bipedal walking. To avoid conflicting control objectives, all aspects of gait control must be tightly integrated. The goal of this thesis is to quantify correlations of parameters that influence the periodic gait. In the course of this, similarities and differences between different control strategies will be analyzed and tested in a bipedal robot simulation. At first, a review of approaches for torso stabilization in bipedal robots will be given. A selected controller will then be implemented and simulated in the given computer model of the JenaFox bipedal walker. Finally, quantitative parameters based on the mechanical cost analysis are determined to evaluate the controller. For this purpose, trajectory optimization is used, to adjust the initial system dynamics in a way that the robot achieves a periodic gait. The designed controller has strong influence of a neural network controller. The concept of vertical leg orientation is used to divide the periodic gait into a phase that repetitively results in a meaningful gait. Finally, a stability analysis is performed, which shows that the gait is asymptotically stable but not energy efficient. Altogether, this thesis investigates control strategies for balancing the trunk in bipedal walking and provides a solution approach that ensures the most periodic gait possible.

Zusammenfassung

Das Ausbalancieren des Rumpfes auf langen Beinen stellt eine große Herausforderung beim zweibeinigen Gehen dar. Um widersprüchliche Steuerungsziele zu vermeiden, müssen alle Aspekte der Gangsteuerung eng miteinander verknüpft werden. Das Ziel dieser Arbeit ist es, Korrelationen von Parametern zu quantifizieren, die den periodischen Gang beeinflussen. Im Zuge dessen werden Gemeinsamkeiten und Unterschiede zwischen verschiedenen Kontrollstrategien analysiert und in einer zweibeinigen Robotersimulation getestet. Zunächst wird ein Überblick über Ansätze zur Torsostabilisierung bei zweibeinigen Robotern gegeben. Ein ausgewählter Regler wird dann in dem gegebenen Computermodell des JenaFox Zweibeiners implementiert und simuliert. Abschließend werden quantitative Parameter auf Basis der mechanical cost analysis ermittelt, um den Regler zu bewerten. Zu diesem Zweck wird eine Trajektorienoptimierung eingesetzt, um die anfängliche Systemdynamik so einzustellen, dass der Roboter einen periodischen Gang erreicht. Der entworfene Regler hat einen starken Einfluss eines neuronalen Netzcontrollers. Das Konzept der vertical leg orientation wird verwendet, um den periodischen Gang in eine Phase zu unterteilen, die wiederholt zu einem sinnvollen Gang führt. Abschließend wird eine Stabilitätsanalyse durchgeführt, die zeigt, dass der Gang zwar asymptotisch stabil, aber nicht energieeffizient ist. Insgesamt werden in dieser Arbeit Regelungsstrategien für das Ausbalancieren des Rumpfes beim zweibeinigen Gehen untersucht und ein Lösungsansatz geliefert, der einen möglichst periodischen Gang gewährleistet.

Contents

Glossary	xiii
Acronyms	xv
1 Introduction	1
2 Fundamentals	3
2.1 Gaits	3
2.1.1 Symmetrical vs. Asymmetrical Gaits	4
2.1.2 Bipedal Gaits	4
2.2 Gait Analysis	5
2.2.1 Spring-Loaded Inverted Pendulum	7
2.2.2 Inverted Pendulum	7
2.2.3 Bipedal Spring-Loaded Inverted Pendulum	7
2.2.4 Virtual Pivot Point	8
2.2.5 Mechanical Cost Analysis	9
2.3 Summary	12
3 Implementation	13
3.1 The JenaFox Bipedal Walking Robot	13
3.2 Neural Network Controller	15
3.3 Vertical Leg Orientation	19
3.4 Trajectory Optimization	20
3.5 Summary	25
4 Evaluation	26
4.1 Stability Analysis	32
4.2 Summary	35
5 Conclusion and future work	36
A Upper and lower bounds of the design variables	37
B Vertical velocity of the center of mass	38
Bibliography	39

List of Figures

2.1	Common gaits of bipeds (a, c) and quadrupeds (b, d). Typical foot contact phases (black and orange dots) are represented as a fraction of stride period on polar plots. The outer ring represents the rear limb contacts (blue) and the inner ring represents the front limb contacts (green). Half a cycle out of phase of fore and hind legs indicates symmetrical gait (a, b), substantial deviations of this in either pair indicates asymmetrical gait (c, d). (Adapted from [26], p. 3)	5
2.2	Schematic representation of the steady-state stance-phase pattern of a bipedal spring-mass model with its characteristic m-shape of the vertical ground reaction force of the right (black) and left (gray) limb. The phase of the double support is shown in blue. One stride period is defined from mid-stance of the left limb to the subsequent mid-stance of the left limb. (Adapted from [26], p. 5)	6
2.3	Schematic representation of the virtual pivot point (VPP), a fixed point on the torso above the center of mass, where the ground reaction force (GRF) is directed to via a hip torque. If the VPP is aligned with the leg, no torso torque is applied and the resulting GRF is directed at the hip joint (a). If the torso is tilted backwards, a negative torso torque (M_{torso}) must be applied to align the GRF with the VPP (b). (Adapted from [29], p. 3)	8
2.4	Schematic representation of the mechanical cost analysis for a compliant spring-loaded inverted pendulum (a) as well as the idealized zero-collision case (b). Shown are the ground reaction force (GRF) and velocity vector \mathbf{v}_{CoM} with their corresponding angles, θ and λ of two isolated, hypothetical strides. The collision angle ϕ is the deviation of the orthogonal relation between the GRF and \mathbf{v}_{CoM} . The collision reduction is quantified by the collision fraction κ . Note that angles and collision fractions are illustrated at specific instances. (Adapted from [24], p. 4)	10
3.1	Schematic representation of the JenaFox bipedal walking robot (a) with its associated coordinate system (b). The bipedal robot consists of a torso connected to two segmented legs, each of which has an upper and a lower link. The abscissa axis (X-axis, orange) points in the direction of motion, the ordinate axis (Y-axis, green) points upward. The trunk of the robot is attached to a boom via a freely rotating joint which constrains the motion of the robot on a sphere. The planar motion is thus restricted to the sagittal plane (i.e. the plane spanned between the abscissa axis and ordinate axis).	14
3.2	The control parameters for the hip (a) extensor $\theta_{ES,h}$ (orange) and flexor $\theta_{FS,h}$ (blue) as well as the knee (b) extensor $\theta_{ES,k}$ (orange) and flexor $\theta_{FS,k}$ (blue) joint angles according to the International Society of Biomechanics convention. (Adapted from [34])	16

3.3	Graphical representation of the four-quadrant inverse tangent, returning values in the closed interval $[-\pi, \pi]$ (a) and alignment of ρ , the angle of the projected velocity vector v_{CH} (blue), and the anterior extreme angle (AEA) (green). Note that the angles are oriented opposite to each other (b).	17
3.4	Linear mapping functions that set the anterior extreme angle (AEA) in direct proportional dependence to ρ	18
3.5	Exponential mapping functions that set the anterior extreme angle (AEA) in exponential dependence to ρ	18
3.6	Sigmoid mapping functions and graphical representation of equation 3.3. The sigmoid function maps the projected velocity vector ρ to obtain the anterior extreme angle (AEA) in a range between -10° and -25°	18
3.7	The bipedal spring mass model for walking. The simulation starts at the moment of vertical leg orientation (VLO) during single support phase (VLO ₀ , green) and ends after one step is completed at VLO of the opposite leg (VLO ₁ , green). The phase of the double support is shown in blue. The trajectory of the center of mass is drawn in orange. (Adapted from [36], p. 1)	20
3.8	Degrees of freedom of the basic mechanical setup. The trunk (mass m_b) has three degrees of freedom (q_1, q_2, q_3), hip and knee of the right leg connect the thigh (m_t) to the body and shank (m_s) to the thigh respectively by one degree of freedom each (q_4, q_5), the same counts for the left side (q_6, q_7). (Adapted from [32], p. 37)	22
3.9	Exponential penalty of the knee angle of the swing leg at touchdown $q_{5, TD}$. Note that the knee is fully extended at $q_{5, TD} = 0^\circ$. The penalty converges to a value of 20.	24
4.1	The collision-based analysis of selected mammals from the literature. Θ , Λ and Φ are shown as a fraction of their sum in a ternary diagram. The filled circles indicate bipedal gaits and the filled squares indicate quadrupedal gaits. The color of the symbols indicate the collision fraction κ with red indicating $\kappa = 1$ and purple $\kappa = 0$ (for spectrum of intermediate colors, see color scale at right). (Adapted from [25], p. 6)	28
4.2	Velocity vectors at touchdown (a) and at VLO ₁ (b). At the beginning of the velocity vectors the leg position is shown schematically, where the hip, knee and ankle joints are drawn as circles. The colors refer to the different motor gains, with red representing the lowest with a GM_h of 1.4, and blue the highest with a GM_h of 1.8. The velocity vectors are scaled by a factor of 0.15.	29
4.3	The trajectory of the horizontal velocity of the center of mass during the motion. For legibility purposes, the first 10s of movement are displayed. The robot moves with an average forward velocity of $0.8379 \frac{m}{s}$. The amplitude of the horizontal velocity ranges from a maximum of $1.7803 \frac{m}{s}$ to a minimum of $-0.7106 \frac{m}{s}$	30
4.4	The angle of the torso (q_3) and the right hip (q_4) with respect to the world from VLO ₀ to VLO ₁ . The phase of the double support is drawn in blue, the time of the touchdown is in the phase change of the single to the double support and is marked by the dashed line (blue). The torso makes a change of direction at the time of the touchdown, i.e. before the touchdown it falls forwards, while falling backwards again after the touchdown.	31
4.5	One cycle of the gait of the JenaFox robot, starting at the moment of VLO ₀ (a) and ending after one step is completed at VLO ₁ of the opposite leg (h).	31

- 4.6 The trajectory of the center of mass (CoM), with the help of which a first impression of the stability can be gained, as bigger oscillations tend to be related with poor robustness of the stability of the gait. The simulation was stopped after a distance of 15 m was reached (a). A more detailed section of the trajectory reveals a negative horizontal displacement at the lower end (b). The horizontal displacement of the torso in [m] is plotted on the abscissa axis, the vertical displacement in [m] on the ordinate axis, respectively. 33
- 4.7 The phase plot of the simulation, i.e. the graphical representation of the behavior of the dynamical system in the phase space over the entire simulation with color-encoded time (a) and ground state (b). The plot shows the position of the torso of the JenaFox robot on the sagittal plane during its motion and reveals that the robot is asymptotically stable in its gait. The vertical displacement of the torso in [m] is plotted on the abscissa axis, the vertical velocity in $\left[\frac{\text{m}}{\text{s}}\right]$ on the ordinate axis, respectively. 34
- B.1 The trajectory of the vertical velocity of the center of mass during the motion. For legibility purposes, the first 10 s of movement are displayed. The average vertical velocity is $-0.0931 \frac{\text{m}}{\text{s}}$. The amplitude of the vertical velocity ranges from a maximum of $0.9501 \frac{\text{m}}{\text{s}}$ to a minimum of $-0.8547 \frac{\text{m}}{\text{s}}$ 38

List of Tables

3.1	Solver settings for the MATLAB [®] Simulink simulation of the JenaFox robot. . .	14
3.2	Overview of the control scheme used for the JenaFox robot. Touchdown (TD) and reaching the anterior extreme angle (AEA) of either hip angle triggers the corresponding action. When the target is reached the power of the moving motors is switched off. In the images, the events are shown as dark stick figures and the corresponding actions as light stick figures. (Adapted from [32], p. 36)	16
3.3	Overview of the used control parameters for the sensory neurons, i.e. the joint angles of the hip extensor $\theta_{ES, h}$ and flexor $\theta_{FS, h}$ as well as the knee extensor $\theta_{ES, k}$ and flexor $\theta_{FS, k}$	19
3.4	Overview of the used control parameters for the motor neurons. τ is a time constant associated with the passive properties of the cell membrane, M_{AMP} represents the magnitude of the servo amplifier. GM_h and GM_k depict the gain of the hip and knee motor, respectively.	19
3.5	Initial conditions used in the multi-body simulation consisting of the knee and hip angles of the swing leg, $q_{5, IC}$ and $q_{4, IC}$, the angle of the torso $q_{3, IC}$ as well as their corresponding velocities $\dot{q}_{5, IC}$, $\dot{q}_{4, IC}$ and $\dot{q}_{3, IC}$. In addition, λ_{IC} , i.e. the initial angle of ν_{CoM} , was passed to the optimizer.	23
3.6	Identified failure modes of the system which may occur. A total of six failure modes were identified, the center of mass (CoM) or one of the knees falling below a threshold in height, the robot starting to walk backwards as well as reaching a time or distance limit. If any of these cases occur, the simulation is aborted and the cost is penalized with a penalty function.	24
4.1	The results of the walking gait.	27
4.2	The results of the mechanical cost analysis.	27
A.1	Upper and lower bounds used in the optimization problem consisting of the initial conditions for the knee and hip angles of the swing leg, $q_{5, IC}$ and $q_{4, IC}$, the angle of the torso $q_{3, IC}$, their corresponding velocities $\dot{q}_{5, IC}$, $\dot{q}_{4, IC}$ and $\dot{q}_{3, IC}$ as well as λ_{IC} , the initial angle of ν_{CoM}	37

Glossary

- Fr Froude number. 10, 27
- GM Motor gain. x, xii, 19, 26, 28, 29
- M Torque (Nm). ix, xiii, 8
- M_{AMP} Magnitude of the servo amplifier. xii, 19
- P_{mech} Power of the limb acting on the center of mass of the body, i.e. the external mechanical power (W). 10
- W_{mech} External mechanical work (J). 10
- Λ Average angle associated with \mathbf{v}_{CoM} relative to horizontal ($^{\circ}$). x, xiii, 11, 12, 27, 28
- Φ Average collision angle ($^{\circ}$). x, xiii, 11, 12, 27, 28
- Θ Average angle associated with the ground reaction force relative to vertical ($^{\circ}$). x, xiii, 11, 12, 27, 28
- α_{TD} Angle of attack ($^{\circ}$). 17, 28
- F_S Spring force (N). 8
- F_T Force associated with M_{torso} (N). 8
- \mathbf{q} Cumulative vector containing the degrees of freedom of the system. 22, 23, 26
- \mathbf{v} Velocity vector ($\frac{m}{s}$). ix, x, xii, xiii, 10, 11, 12, 16, 17, 19, 22, 23, 24, 26, 27, 28, 36, 37
- κ Collision fraction, calculated as the quotient of Φ and the sum of Θ and Λ . ix, x, 10, 12, 27, 28
- λ Instantaneous angle of \mathbf{v}_{CoM} relative to horizontal ($^{\circ}$). ix, xii, 9, 10, 11, 12, 19, 22, 23, 37
- ϕ Instantaneous angle of deviation of perpendicularity of force and velocity vectors (collision angle) ($^{\circ}$). ix, 9, 10, 11, 12
- ρ Angle of \mathbf{v}_{CH} relative to horizontal at touchdown ($^{\circ}$). x, 17, 18, 26, 36
- τ Time constant associated with the passive properties of the cell membrane (s). xii, 19
- θ Instantaneous angle of the ground reaction force relative to vertical ($^{\circ}$). ix, 9, 10, 11, 12
- θ_{ES} Control parameter of the extensor for the neural controller ($^{\circ}$). ix, xii, 16, 19, 26
- θ_{FS} Control parameter of the flexor for the neural controller ($^{\circ}$). ix, xii, 16, 19, 26
- d Offset, i.e. a shift of the function along the abscissa axis. 18

g Acceleration due to gravity ($\frac{\text{m}}{\text{s}^2}$). 10, 11

k Constant of proportionality, which relates two variables in a direct variation. 18

m Mass of the body (kg). 11

t Simulation time (s). 6, 23, 24, 27, 36

x Horizontal displacement (m). 20, 24, 27, 28, 29

y Vertical displacement (m). 10, 11, 17, 24, 27, 32

Acronyms

GRF Ground Reaction Force ix, xiii, 6, 7, 8, 10, 11, 12

AEA Anterior Extreme Angle x, xii, 15, 16, 17, 18, 19, 26, 36

BSLIP Bipedal Spring-Loaded Inverted Pendulum 6, 7

CoM Center of Mass ix, x, xi, xii, xiii, 3, 6, 7, 8, 9, 10, 11, 12, 16, 17, 19, 20, 22, 23, 24, 27, 28, 29, 30, 32, 33, 36, 37, 38

CoT Cost of Transport 1, 24, 36

CoT_{mech} Mechanical Cost of Transport 1, 2, 9, 11, 27, 35

DoF Degrees of Freedom xiii, 8, 22

IP Inverted Pendulum 3, 6, 7, 8, 12, 15

ISB International Society of Biomechanics ix, 16

MCA Mechanical Cost Analysis v, ix, xii, 2, 4, 6, 9, 10, 12, 26, 27, 35

NLP Nonlinear Program 21, 24, 36

ODE Ordinary Differential Equation 14, 36

PEA Posterior Extreme Angle 16

SLIP Spring-Loaded Inverted Pendulum ix, 3, 6, 7, 9, 10, 12

TUM Technical University of Munich iii

VLO Vertical Leg Orientation v, x, 13, 19, 20, 21, 22, 23, 24, 25, 28, 29, 30, 31

VPP Virtual Pivot Point ix, 6, 8

Chapter 1

Introduction

Robotics aims to build artificial cognitive systems that can act on their own to achieve some predefined goal. However, in order to be able to respond to and interact with one's environment, it is necessary to grasp the basic mechanisms of our world. To master this, agents¹ are required to perceive their environment, anticipate the need to act, learn from experience, and adapt to changing circumstances. In order to be able to perform tasks imposed by humans, mobile robots must navigate a complex, uncertain, unstructured and human-shaped environment. This can only be achieved by exhibiting some degree of cognition. [40] Hereby, nature provides a remedy. The course of millions of years of evolution created an almost inexhaustible arsenal of potential solutions and highly optimized system processes, which frequently inspire engineers. [37]

Studies of mechatronic systems inspired by biology can be categorized in respects of locomotion and mechanisms, actuation, sensing, and control [38]. Especially nature's ways of mastering locomotion provide a myriad of inspirations as nature has evolved various biological forms and functions to maneuver energy efficiently, agilely and safely through even the most hazardous environments. Locomotion is equally fundamental to all living things for foraging, catching prey, evading predators, protecting territory, finding mates, and migrating. For mankind in particular, it has played a central role in hunting, agriculture, transportation, sports, and warfare. [26] As with any structurally or functionally occurring feature in nature, it is important to observe locomotion through the lens of organic evolution, as it emerged through the process of natural selection rather than through the mostly straightforward process of engineering. Subsequently, two main types of terrestrial legged locomotion have established in nature: walking upright on at least two legs like humans and most mammals do, which facilitates fast locomotion; and crawling low over the ground like reptiles, which usually tends to greater stability especially on rough terrain. [38] Hereby, energy comes at a premium not only for living creatures but also for robots, which need to carry sufficient energy in their batteries. Although the energy of a robot is consumed at many levels, from the control systems to the actuators, Lee and Harris [26] assume that the mechanical cost of transport (CoT_{mech}) is an integral energy cost. Measuring this consumption allows the most direct comparison between the gaits of legged creatures and robots. Although legged robots have equaled or even surpassed the total cost of transport (CoT) of legged creatures, this is usually only achieved by choosing extremely slow speeds or by using regenerative mechanisms. [26]

The goal of this work is to stabilize the torso of a bipedal robot and thus enable free movement of the upper body on a plane, as the trunk was previously fixed with rather stiff

¹Respectively any artificial entity displaying some degree of cognition [40].

springs and hence unable to swing forward or backward with previous walking patterns. In the course of this, correlations of parameters that influence the periodic gait shall be found. By simulating and analyzing the dynamics of the entire system, an attempt is made to deduce a control law. In order to be able to select a suitable method, it is necessary to understand which gait types have established in nature, their characteristics and how they can be distinguished. Chapter 2 gives an overview of this and then presents different possibilities, from which the mechanical cost analysis (MCA) has emerged as the most promising approach and is thus pursued further. Subsequently, a biologically inspired controller is implemented, with the help of which a periodic gait can be achieved. The robot, controller, and further methods used are presented in chapter 3. Finally, quantitative parameters based on the MCA, which include the previously mentioned CoT_{mech} , are determined to evaluate the controller. The results are presented in chapter 4. Since a periodic although not energy efficient gait was found, an outlook with possible improvements is given in the final chapter 5.

Chapter 2

Fundamentals

Over millions of years of evolution, living creatures have developed various modes of locomotion, so-called gaits, which can be distinguished by their movement. For example, locomotion patterns with legs can be categorized via temporary footfall patterns. The analysis of terrestrial legged locomotion in the last half century has focused mainly on strategies for mechanical energy recovery during walking and running [24]. Two pioneers of kinematic measurement are Étienne-Jules Marey (1830 - 1904) and Eadweard Muybridge (1830 - 1904). The former published studies on the movements of human limbs as early as 1873, while the latter became famous by demonstrating that a horse at a trot lifts all four of its feet off the ground simultaneously at certain times. [3] In the mid-1960s, Hildebrand [16] and others used cine films at a frame rate of 128 and 64 fps to distinguish gaits of terrestrial legged animals by such means as the duty cycle or limb contact phases. About a decade later, Cavagna, Heglund, and Taylor [6] revolutionized the understanding of animal locomotion by defining center of mass (CoM) mechanics using a point mass model and force plate measurements of the whole animal. Their comparison of walking and running reduced gait complexity by proposing that separate and mutually exclusive mechanisms act to exchange energy during the gait phase, such as anti-phase to in-phase kinetics and potential energy fluctuations. The same authors induced today's widely accepted paradigm of conceptualizing walking as an inverted pendulum (IP) and running as a compliant spring-loaded inverted pendulum (SLIP). [25] While walking, the mechanical energy of the CoM remains nearly constant while kinetic and potential energies interchange oscillatorily, causing the CoM to ascend over the supporting limb in mid-stance and fall forward into the next step. During running, however, this exchange is not possible because the CoM attains its lowest point in mid-stance, where the kinetic energy is also low. For this reason, running gaits are assumed as a spring-mass mechanism in which the interaction between the CoM and the ground allows for the storage and return of elastic strain energy in rather compliant legs. [24]

2.1 Gaits

One way to identify the gait of terrestrial legged animals is by their footfall sequence. Gaits can be quantified by the phase relationship of the individual legs and expressed as a fraction or percentage of the time of foot contact to the stride¹ period. For example, in bipedal walking, one foot lands at the beginning of the stride (i.e. at 0%) and the second foot lands at mid-stride (i.e. at 50%), representing one entire step. However, a phase-based definition of gait is often incomplete and may result in an inability to distinguish between different gaits because they may have similar or even identical phase relationships. For example,

¹A stride consists of two consecutive steps.

bipedal walking (see figure 2.1a, black) and running (see figure 2.1a, orange) share the same left-right-left sequence of footfalls, with the phases of first contact of the alternating feet at 0% and 50% of the stride period, respectively. Therefore, the distinction between walking and running has traditionally been based on the duty factor, which represents the duration of a given footfall as a fraction of the stride period. On this basis, human running and walking can be distinguished, as human running has a defined duty factor of <0.5 , which specifies a distinct air phase. However, in multi-legged running the steps with duty factor <0.5 can follow each other in such a way that there is no air phase. Furthermore, considering birds, the difference between running and walking becomes blurred, as they exhibit "grounded" running with no air phase when the duty factor is >0.5 . Although the distinction between running and walking based on the duty factor is very straightforward, criteria beyond temporal footfall metrics, such as evaluating gaits via MCA, are needed to distinguish the underlying physics of gait. [26] For that purpose, Lee et al. [24] provided the first experimental evidence in 2011 showing that a collision-based approach can differentiate quadrupedal gaits and quantify interspecific differences. The following two sections give insight into the distinction between symmetric and asymmetric gaits as well as bipedal gaits, which, however, contrary to what was assumed at the beginning of this thesis, is not of great importance in the further course of this work.

2.1.1 Symmetrical vs. Asymmetrical Gaits

Legged gaits can be classified as symmetrical and asymmetrical, according to the phase relationship of the left-right pairs of legs, regardless of the number of pairs. If the left and right leg of a pair are out of phase by half a stride, the gait is defined as symmetrical - if not, the gait is defined as asymmetrical. Examples of a symmetrical gait include the bipedal walking of humans, the quadrupedal trotting of dogs, the pacing of camels, and the six-legged trotting of cockroaches, where all left-right pairs of front, middle, and hind legs are one-half stride cycle out of phase with one another. The number of legs limits the number of leg sequencing options, such that bipedal striding gaits are restricted to symmetric (walking (black) and running (orange), see figure 2.1a) and asymmetric gaits (skipping (black) and hopping (orange), see figure 2.1c). Quadrupeds use five symmetrical gaits (lateral and provisional diagonal sequence walking (black), trotting (orange, see figure 2.1b), pacing and ambling) and six asymmetrical gaits (lope, transverse and rotary gallops (black), half-bound (orange, see figure 2.1d), bound, and pronk). [26] However, note that these are broad definitions and that phase separations between foot contacts show substantial variation within gaits, as can be seen in Hildebrand's plots ([16] [17]) for the gaits of horses and dogs. In summary, the difference between symmetrical and asymmetrical gaits lies in the coordination of the legs, with symmetrical gaits involving both legs on the same side moving together and asymmetrical gaits involving diagonally opposite pairs of legs moving together.

2.1.2 Bipedal Gaits

Bipedal striding gaits, including that of humans, are symmetrical by definition (see figure 2.1a). Biomechanically, bipedal gaits involve the coordinated movement of multiple joints, including the ankle, knee, and hip, as well as the interaction of the musculoskeletal system and the central nervous system. The foot must make contact with the ground in a manner that provides stability and propulsive forces, while also allowing for the transfer of energy from one limb to the other. These gaits can be found today mainly in birds and in earlier times in theropod dinosaurs, which also represent the greatest diversity of bipedal

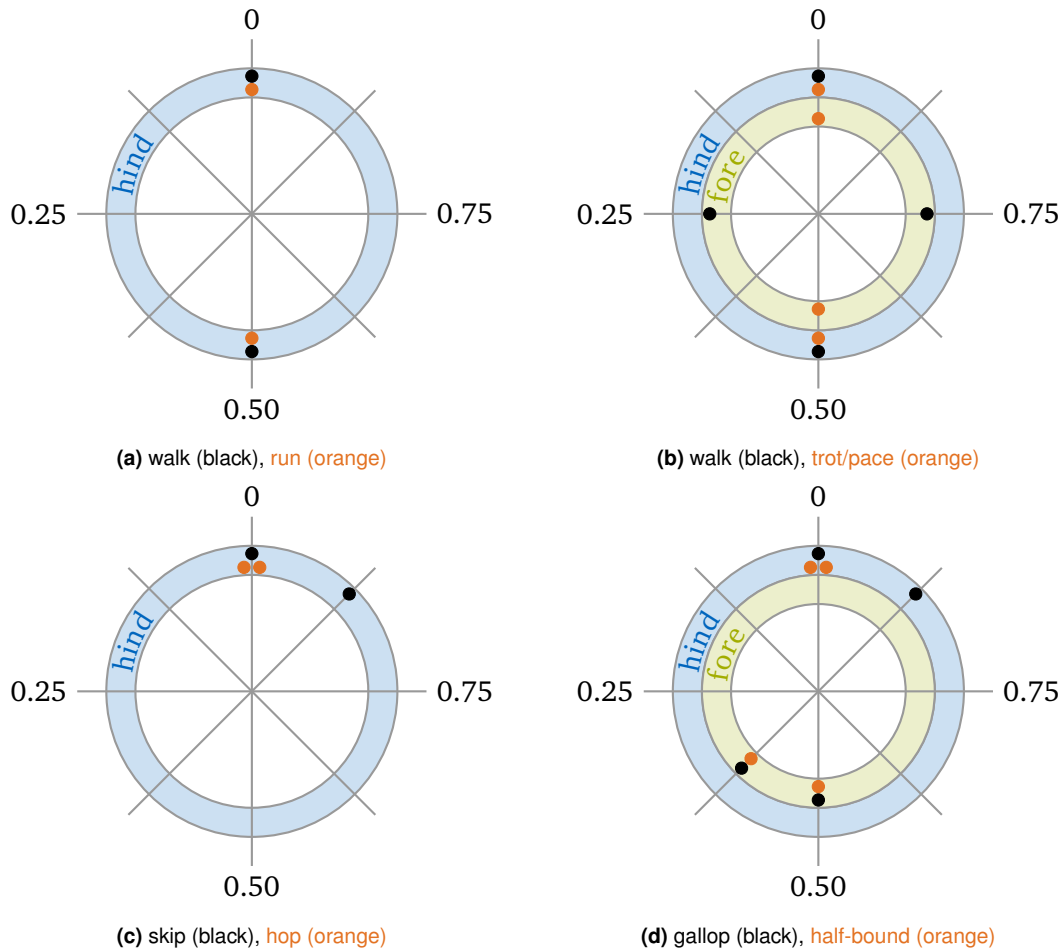


Figure 2.1: Common gaits of bipeds (a, c) and quadrupeds (b, d). Typical foot contact phases (black and orange dots) are represented as a fraction of stride period on polar plots. The outer ring represents the rear limb contacts (blue) and the inner ring represents the front limb contacts (green). Half a cycle out of phase of fore and hind legs indicates symmetrical gait (a, b), substantial deviations of this in either pair indicates asymmetrical gait (c, d). (Adapted from [26], p. 3)

runners. Humans and most birds² walk at slow speeds and run at fast speeds. [26] Some great apes and monkeys are volitional bipeds, but usually only for rather short distances. At top speed, some lizards [19] and cockroaches [8] can bring their bodies into an almost upright posture and thus achieve bipedal running movements, increasing speed by expanding stride length. In general, bipeds achieve greater absolute stride lengths than quadrupeds of the same body mass [35]. This has been argued to be an advantage for endurance runners as our own species, for example while engaging in persistence hunting quadrupeds or aggressive scavenging in competition with them [5].

2.2 Gait Analysis

In order to be able to evaluate the performance of a given gait, different analysis techniques can be used. Gait analysis is the systematic study of walking patterns and movements, with the goal of understanding the mechanics of walking and, in the field of robotics, developing control algorithms to improve the robot's stability and balance. From a motor control

²Except small songbirds, which typically have more of a hopping than walking gait [26].

perspective, bipedal gaits are thought to be controlled by a combination of reflexive and voluntary mechanisms, with the former providing stability and the latter allowing for intentional changes in gait patterns [15]. A wide variety of models has been developed to analyze terrestrial legged locomotion, which can be classified based on the phase relationship of the kinetic and potential energy oscillations. Two of the most influential models for gait analysis for bipedal, quadrupedal, and multi-legged locomotion are the spring-loaded inverted pendulum (SLIP) and the inverted pendulum (IP) models. [26] Both methods model the subject as a point mass with oscillating massless legs, which allows the neglect of rotations around the CoM [20]. In bipedal gaits, the leading foot represents the braking force and serves as an anchor point for the body's next movement. Contrary to that, the trailing foot represents the propulsive force that adds energy to the system to vault over this same anchor point. In mid-stance, the CoM reaches its lowest point when running, i.e. the minimum potential energy, and the provisional highest point when walking, i.e. the maximum potential energy. Since braking occurs in the first half of a leg's stance phase and propulsion in the second half, the CoM velocity, i.e. the kinetic energy, reaches its minimum at mid-stance for both walking and running. [26] Figure 2.2 shows a schematic representation of the characteristic m-shape of the vertical ground reaction force (*GRF*) of a steady-state stance-phase pattern of a bipedal spring-mass model. The following sections give insight about the previously mentioned SLIP and IP models. Furthermore, the bipedal spring-loaded inverted pendulum (BSLIP) model, an alternative walking model for compliant legs, and the virtual pivot point (VPP), a concept to analyze mechanical systems, are touched upon. At the beginning of this thesis, these methods were considered to be used, but as the work progressed, it quickly became apparent that the MCA would be pursued.

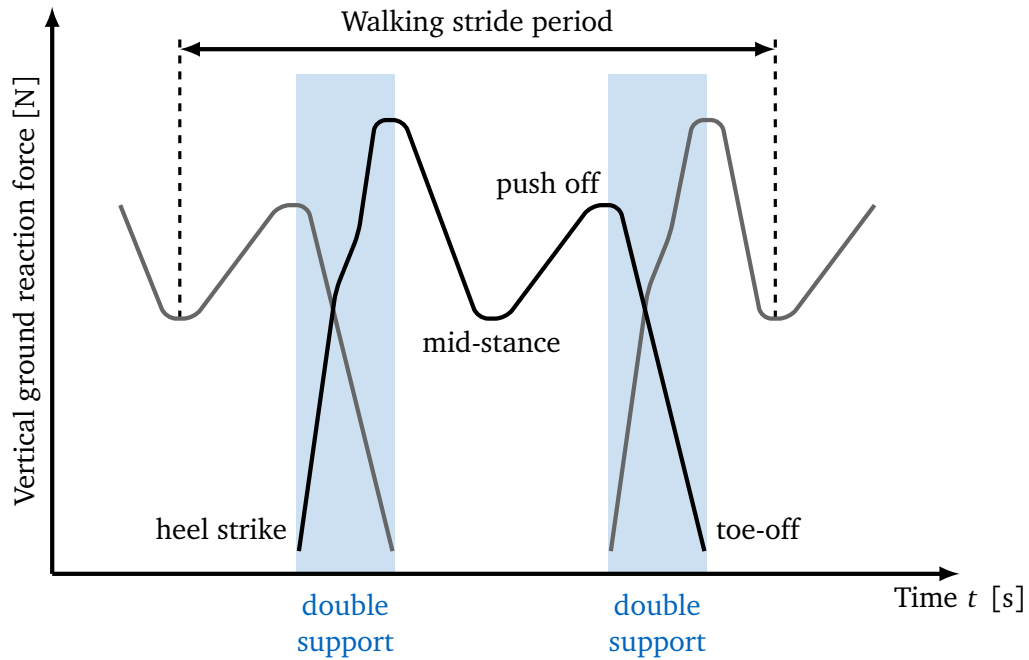


Figure 2.2: Schematic representation of the steady-state stance-phase pattern of a bipedal spring-mass model with its characteristic m-shape of the vertical ground reaction force of the right (black) and left (gray) limb. The phase of the double support is shown in blue. One stride period is defined from mid-stance of the left limb to the subsequent mid-stance of the left limb. (Adapted from [26], p. 5)

2.2.1 Spring-Loaded Inverted Pendulum

The SLIP model represents a spring-mass system, where a pendulum represents the body of a walker mounted on a spring and supported by the **GRF**. The pendulum, i.e. the CoM of the body, is assumed as a point mass, and the massless spring serves as the ankle joint and its associated muscles and tendons in the legs. The model treats the phase of the stride in which the CoM is vaulting over the stance foot as an inverted pendulum with springs added inline to the legs. Since the springs are able to store energy during collision with the ground (i.e. during heel strike) and return it to the CoM during toe off, this model is typically found in running gaits. [4] SLIP-like gaits include bipedal running and hopping, as well as quadrupedal and multi-legged trotting, often described as "bouncing" gaits as the greatest leg compression occurs at about the same time as the greatest vertical force [30]. This spring-based gait can also be seen in animals that frequently hop, such as kangaroos. When physical springs are present, energy savings can be achieved via elastic storage and proportional return of absorbing and generative work performed by muscles or actuators. Overall, the SLIP model is a simple, yet quantitative way to represent the dynamics involved in walking and running and to analyze the energy economy describing the mechanical work done by the muscles and tendons. [4]

2.2.2 Inverted Pendulum

In the IP model the body of the walker is represented as a rigid rod that is inverted and balanced on a pivot point. The rod represents the body's CoM, and the pivot point represents the ankle joint. The body is subjected to gravitational forces that cause it to oscillate back and forth as it moves forward. According to the conventional interpretation of "two basic mechanisms", which states that the potential energy tends to reach a maximum near mid-stance during walking, it is sufficient to describe walking dynamics with an IP model derived using Lagrangian mechanics and non-linear equations of motion. The system is considered to be under-actuated because the control inputs are limited to the forces and torques at the ankle and knee joints. [26] Nonetheless, experimental studies show that bipedal and quadrupedal walking dynamics (e.g. [23], [14], [11]) are not well reflected by the IP model. This is unsurprising given that an actual rigid inverted pendulum (i.e., a mass on a massless rod of fixed length) would show a peak vertical force instead of a minimum vertical force in the mid-stance position, as described by Geyer, Seyfarth, and Blickhan [12]. The authors presented an alternative walking model for compliant legs, called the bipedal spring-loaded inverted pendulum model, which is described in more detail in the following section.

2.2.3 Bipedal Spring-Loaded Inverted Pendulum

The BSLIP model, proposed by Geyer, Seyfarth, and Blickhan, is a variation of the SLIP model specifically designed to study bipedal walking gaits. The model is able to reproduce a similar m-shape of the vertical **GRF** as shown in figure 2.2 by providing a spring-loaded leg that introduces compliance. In addition, the model aggregates the leading and trailing leg forces during double support of the step-to-step transition. Although the BSLIP model is widely used and frequently cited, it has not yet challenged the IP model in most textbooks. This may be in part because the BSLIP is more difficult to simulate and perhaps also because its conservative leg springs limit its ability to achieve the full range of human walking speeds. [27] Nevertheless, SLIP-like running and BSLIP-like walking were successfully demonstrated on a bipedal robot using the same spring-loaded legs for both gaits [18]. Theoretically, the BSLIP

represents a more lifelike model because, unlike the rather unrealistic impulsive stride-to-stride transition of the IP model, it is able to capture the characteristic m-shape of the **GRF** profile and, moreover, allows for double support [26].

2.2.4 Virtual Pivot Point

The VPP is a concept used to analyze mechanical systems with multiple degrees of freedom (DoF). The VPP depicts a hypothetical point in a mechanical system that behaves as if it is a fixed pivot point, even though it is not actually fixed. This point can then be used as a reference point for analyzing the motion of other parts of the system. The position of the VPP is typically chosen based on the geometry and dynamics of the system. [29] For the analysis of bipedal gaits, the VPP can be chosen as a fixed point on the torso above the CoM, where the **GRF** is directed to via a hip torque, which allows to take the position of the leg into account. [39] If the VPP is aligned with the leg, no torso torque is applied and the resulting **GRF** is directed at the hip joint, as shown in figure 2.3a. However, if the torso is tilted backwards, a negative torso torque must be applied to align the **GRF** with the VPP, as can be seen in figure 2.3b. [29] When the **GRF** always directs at the VPP it becomes a virtual hinge around which the torso will rotate, which transforms the difficult task of balancing an inverted pendulum to a system consisting of a pendulum suspended from a hinge, which is intrinsically stable. [39]

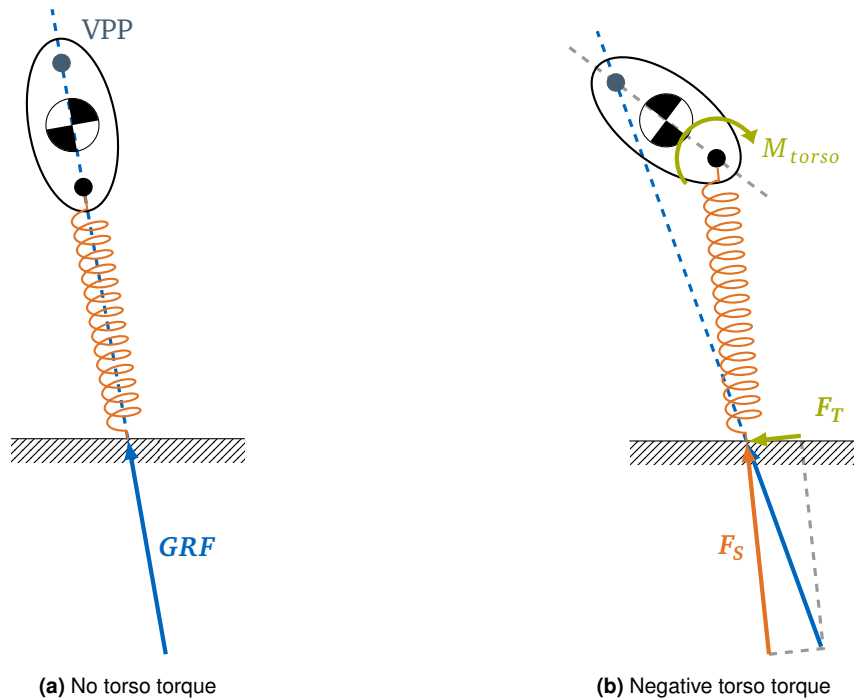


Figure 2.3: Schematic representation of the virtual pivot point (VPP), a fixed point on the torso above the center of mass, where the ground reaction force (**GRF**) is directed to via a hip torque. If the VPP is aligned with the leg, no torso torque is applied and the resulting **GRF** is directed at the hip joint (a). If the torso is tilted backwards, a negative torso torque (M_{torso}) must be applied to align the **GRF** with the VPP (b). (Adapted from [29], p. 3)

2.2.5 Mechanical Cost Analysis

The MCA is a method used to quantify the energy consumption and efficiency of movement patterns in biological and artificial systems. The goal of this analysis is to quantify the amount of energy required to perform a given task, such as walking or running, and to understand how different factors, such as speed, terrain, and body size, influence the energy cost. It involves calculating and comparing the mechanical work done by the system, i.e. the force applied to and the displacement of the system, as well as the metabolic energy consumption, to quantify the overall efficiency of the movement. MCA is widely used in fields such as biomechanics, sports science, and robotics where it is important to understand the energy consumption and efficiency of movement patterns. In biomechanics, MCA can be used to study the energy consumption of different walking styles, while in robotics it can be used to optimize the energy efficiency of movements. The CoT_{mech} can be decomposed into several components, including the work done against gravitational forces, work done against inertial forces, work done against frictional forces, and work done to change the velocity of the body segments. These components can be calculated using principles from mechanics, such as work-energy, impulse-momentum, and conservation of energy. The CoT_{mech} can also be influenced by various factors, such as body size and shape, limb coordination, and actuator activation patterns. For example, taller agents generally have a higher CoT_{mech} than shorter individuals just because they have to overcome larger gravitational forces. [2]

Based on this Lee et al. [24] developed a collision-based approach, which uses the same point mass model as SLIP-based methods, but describes the locomotion directly by analyzing the force and velocity vectors. Unlike SLIP-based approaches, which are only approximations of a gait, the collision-based approach has the advantage that no *a priori* model needs to be known, which holds the potential to distinguish different gaits as well as to discern their defined characteristics [24].

Fundamental Determinants of Center of Mass Dynamics

The central concept of MCA is D'Alembert's 'principle of orthogonal constraint', which shows that a mass can be redirected without mechanical work, as long as the constraint (i.e. the force vector) is perpendicular to the path (i.e. the velocity vector), such that their dot-product (i.e. the mechanical power) is zero. However, this theoretical redirection with zero work cannot be implemented in real legged systems as terrestrial legged locomotion requires intermittent, discrete footfalls. Among other things, this constrains the system's ability to exert orthogonal forces by a leg's position with respect to the CoM, their kinematic range of motion and their force-torque capacity. [26] These "inelastic" collisions [22] by the limb with the ground preclude a consistent orthogonal relationship between the force and velocity vector, as their corresponding instantaneous angles θ (relative to vertical) and λ (relative to horizontal) [25] are of the same sign³, as shown in Figure 2.4a. This results in a non-zero collision angle ϕ and abrupt, collision-like changes in the CoM direction, which require mechanical work [24]. However, in the theoretical case, if the two vectors are perpendicular to each other, $\phi = 0$, meaning the angles θ and λ are equal and of opposite sign, which in turn means that no collision occurs, and no work is done at the CoM, as for a wheel without rim but infinite spokes [2]. A schematic representation of this concept is shown in figure 2.4b.

³This is consistent with compliant SLIP mechanics [25].

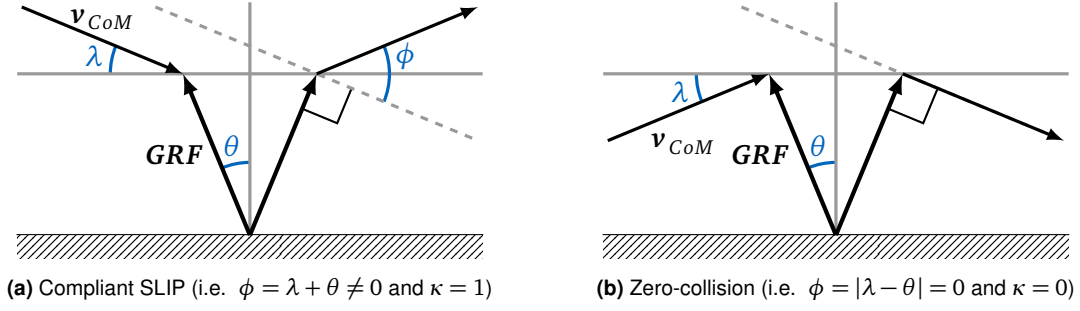


Figure 2.4: Schematic representation of the mechanical cost analysis for a compliant spring-loaded inverted pendulum (a) as well as the idealized zero-collision case (b). Shown are the ground reaction force (**GRF**) and velocity vector \mathbf{v}_{CoM} with their corresponding angles, θ and λ of two isolated, hypothetical strides. The collision angle ϕ is the deviation of the orthogonal relation between the **GRF** and \mathbf{v}_{CoM} . The collision reduction is quantified by the collision fraction κ . Note that angles and collision fractions are illustrated at specific instances. (Adapted from [24], p. 4)

To enforce the principle of orthogonal constraint, that is, to keep the force and velocity vectors of the CoM as orthogonal as possible, both metrics must be measured at each instant of the stride. If this orthogonal relationship is violated, either generative or absorptive costs are incurred, depending on the sign of the collision angle ϕ , which is the summation of the force and velocity angles θ and λ . If $\phi < 90^\circ$, the cost is generative, i.e., the two vectors point somewhat in the same direction and energy can be applied to move forward. Conversely, if $\phi > 90^\circ$, the cost and energy are absorptive, as is the case with deceleration. Theoretically, provided both vectors are always exactly 90° out of phase, it would hereby be possible to redirect the CoM with zero work. [26] The power of the limb acting on the CoM of the body, i.e. the external mechanical power, can thus be quantified as

$$P_{mech} = \mathbf{GRF} \cdot \mathbf{v}_{CoM} \sin(\phi) \quad (2.1)$$

where **GRF** denotes the respective force vector, i.e. the external force acting on the limb, and \mathbf{v}_{CoM} the velocity vector of the CoM. The mechanical work performed corresponds to the cumulative time integral over the duration of the impulse of the external mechanical power [7] [24]:

$$W_{mech} = \int P_{mech} dt. \quad (2.2)$$

Center of Mass Velocities

A common dimensionless unit for comparing moving objects is the Froude number (Fr). It can be used to classify walking gaits into different categories based on the relative importance of inertial and gravitational forces in the motion of the body. For example, when $Fr < 1$, the walking gait is characterized by stability-seeking behavior, while when $Fr > 1$, the walking gait is characterized by energy-saving behavior. The dimensionless velocity is the square-root of the Froude number [1] [24]

$$\sqrt{Fr} = \sqrt{\frac{\mathbf{v}_{CoM_x}^2}{g \cdot y_{CoM}}} = \frac{\mathbf{v}_{CoM_x}}{\sqrt{g \cdot y_{CoM}}} \quad (2.3)$$

where $\overline{v_{CoM_x}}$ depicts the average forward velocity, g the acceleration due to gravity and y_{CoM} the vertical displacement of the CoM of the body.

Collision-Based Angles

The instantaneous collision angle ϕ is the deviation of perpendicularity of force and velocity vectors of the CoM [24], which is measured at each instance of the step and given by the dot product of force on velocity

$$\phi = \arcsin\left(\frac{|\mathbf{GRF} \cdot \mathbf{v}_{CoM}|}{|\mathbf{GRF}| |\mathbf{v}_{CoM}|}\right). \quad (2.4)$$

The arcsine represents a phase shift of $\frac{\pi}{2}$ to define an angle of zero when the force and velocity vectors are perpendicular to each other. Note that ϕ is undefined during flight periods, i.e. when $\mathbf{GRF} = 0$. The instantaneous velocity angle with respect to the horizontal λ and the instantaneous force angle with respect to the vertical θ [24] are given by

$$\lambda = \arccos\left(\frac{|\mathbf{v}_{CoM_x}|}{|\mathbf{v}_{CoM}|}\right) \quad (2.5)$$

$$\theta = \arccos\left(\frac{|\mathbf{GRF}_y|}{|\mathbf{GRF}|}\right). \quad (2.6)$$

The collision angle over the contact periods of the entire stride Φ is given by the weighted average of ϕ , where the weights represent the magnitude of the force and velocity vectors at each instant [24]:

$$\Phi = \frac{\sum |\mathbf{GRF}| |\mathbf{v}_{CoM}| \phi}{\sum |\mathbf{GRF}| |\mathbf{v}_{CoM}|}. \quad (2.7)$$

Similarly, the stride velocity angle with respect to the horizontal Λ and the stride force angle with respect to the vertical Θ can be determined from instantaneous velocity and force angles, λ and θ , respectively [24]:

$$\Lambda = \frac{\sum |\mathbf{v}_{CoM}| \lambda}{\sum |\mathbf{v}_{CoM}|} \quad (2.8)$$

$$\Theta = \frac{\sum |\mathbf{GRF}| \theta}{\sum |\mathbf{GRF}|}. \quad (2.9)$$

Applying the small angle approximation of equation 2.4 in equation 2.7, that is, when only small vertical undulations and fore-aft forces appear, shows that the collision angle Φ is a close approximation to the CoT_{mech} [24] if $\sin(\phi) \approx \phi$ (i.e. if ϕ is less than about 0.3 rad), as can be seen in

$$\Phi \approx \frac{\sum |\mathbf{GRF} \cdot \mathbf{v}_{CoM}|}{\sum |\mathbf{GRF}| |\mathbf{v}_{CoM}|} \approx \text{CoT}_{\text{mech}} = \frac{\sum |\mathbf{GRF} \cdot \mathbf{v}_{CoM}|}{\overline{v_{CoM_x}} m g} \quad (2.10)$$

where the CoT_{mech} is a dimensionless metric of the normalized mechanical power during the contact period of the gait when the limb redirects the CoM [25], i.e. the mechanical work at the CoM required to move a unit body weight a unit distance in the direction of travel [24] [6].

Collision Fraction

The collision reduction is directly correlated to the collision angle Φ and quantified by the collision fraction κ , which gets small if either the velocity angle Λ^4 or the force angle Θ is small, if there is a near perpendicularity of the velocity vector \mathbf{v}_{CoM} and the **GRF** throughout the stride or any combination thereof. The collision fraction is the actual collision relative to potential collision:

$$\kappa = \frac{\sum |\mathbf{GRF}| |\mathbf{v}_{CoM}| (\phi / (\theta + \lambda))}{\sum |\mathbf{GRF}| |\mathbf{v}_{CoM}|} = \frac{\Phi}{\Theta + \Lambda}. \quad (2.11)$$

For the compliant SLIP, $\phi = \lambda + \theta \neq 0$ and $\kappa = 1$, since the braking force yields a non-perpendicular angle with downward velocity whereas the propulsive force yields one with upward velocity (see figure 2.4a), which occurs whenever the **GRF** and \mathbf{v}_{CoM} are oriented in opposite directions from the vertical and horizontal axes. Whenever the **GRF** and \mathbf{v}_{CoM} are oriented in the same direction, collisions are reduced and $\kappa < 1$ up to the idealized case in which the **GRF** and \mathbf{v}_{CoM} remain orthogonal throughout the entire stride and thus $\phi = |\lambda - \theta| = 0$ and $\kappa = 0$, as shown in figure 2.4b. Note that for a geometrical representation angles and collision fractions are illustrated at specific instances. [24]

2.3 Summary

Locomotion is equally fundamental to all living things. Nature provides a myriad of various biological forms and functions to maneuver energy efficiently, agilely and safely through even the most hazardous environments, which evolved over the course of millions of years of evolution. [26] The analysis of terrestrial legged locomotion in the last half century has focused mainly on strategies for mechanical energy recovery during walking and running [24]. Legged locomotion can be classified in symmetrical and asymmetrical gaits, according to the phase relationship of the left-right pairs of legs, regardless of the number of pairs. A common definition depicts that symmetrical gaits involve both legs on the same side moving together whereas asymmetrical gaits involve diagonally opposite pairs of legs moving together. Models have been developed to further analyze terrestrial legged locomotion and can be classified based on the phase relationship of the kinetic and potential energy oscillations. Two of the most influential models for gait analysis for bipedal, quadrupedal, and multi-legged locomotion are the spring-loaded inverted pendulum (SLIP) model for running, where the energy oscillations are in phase, i.e. the kinetic and potential energy both reach a minimum at mid-stance, and the inverted pendulum (IP) model for walking, where the energy oscillations are out of phase. [26] Energy consumption and efficiency of movement patterns in biological and artificial systems can be quantified with the mechanical cost analysis (MCA). This method involves calculating and comparing the mechanical work done by the system, i.e. the force applied to and the displacement of the system, as well as the metabolic energy consumption, to quantify the overall efficiency of the movement. [2]

⁴Which tends to be greater in SLIP-like gaits such as running, hopping or trotting due to increased vertical oscillations of the CoM during these "bouncing" gaits [25].

Chapter 3

Implementation

A MATLAB® Simulink [28] implementation of the JenaFox model, reflecting the test environment described in the upcoming section 3.1, was provided. A modified neural network controller based on the work of Geng, Porr, and Wörgötter [10] was used as a controller, which is discussed in more detail in section 3.2. The concept of vertical leg orientation (VLO), proposed by Rummel et al. [36] and described in section 3.3, was taken as initial and final condition, i.e. one iteration of the simulation consists of one full step or one half of a stride, respectively. The iterations were finally analyzed using a trajectory optimization, described in section 3.4, in order to achieve a solution that is as periodic as possible, in other words, with as little difference as possible between the final and initial conditions of the robot.

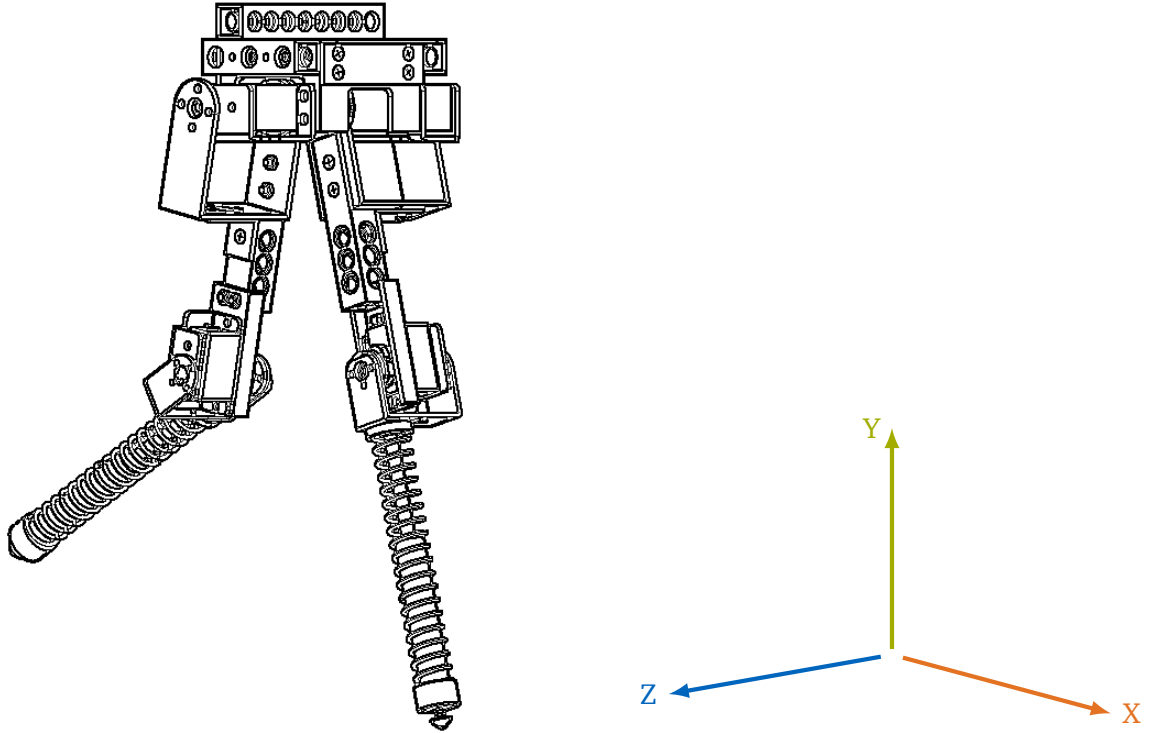
3.1 The JenaFox Bipedal Walking Robot

JenaFox refers to a bipedal robot developed at the Friedrich-Schiller-University Jena in Germany, designed for research in robotics and control engineering with a focus on bipedal locomotion. The robot resembles two human-like legs, connected by a torso, that are capable of walking and navigating different terrains. The system is equipped with a variety of sensors, such as accelerometers and gyroscopes, which provide data on its motion and orientation. This data can then be used to control the robot's actuators and thus its movements, allowing it to balance, walk, and respond to its environment in real-time. The robot is also designed to be highly scalable and modular, with a wide range of interchangeable components that can be customized to meet specific research needs. This includes the ability to easily swap out different sensors, actuators, and control boards, allowing researchers to easily experiment with different configurations and components. [31]

The robotic test environment is unique in that it is designed as an open-source platform, making it accessible to researchers and students who want to study and experiment with bipedal robotics. Overall, JenaFox is a valuable tool for researchers and students in the field of robotics and control engineering, as it provides a platform for exploring the challenges and opportunities associated with bipedal locomotion, and for developing new technologies and control strategies for robots. [31]

A schematic representation of the JenaFox robot is shown in figure 3.1a. The bipedal robot consists of a torso connected to two segmented legs, each of which has an upper and a lower link. When taking a step, the stance leg supports the weight of the robot, while the swing leg is free to move above the ground. All limbs are connected via actuators, with sensors in each joint measuring angular position and velocity, except for the ankle joint, which is

the only passive joint of the system. The trunk of the robot is attached to a boom via a freely rotating joint. The tether mechanism constrains the motion of the robot on a sphere, without excessively affecting its dynamics in the sagittal plane (i.e. the plane spanned between the abscissa axis (X-axis, orange) and ordinate axis (Y-axis, green), see figure 3.1b). The mechanism consists of an aluminum tube, a spherical pivot fixed to the floor and a tension cable. The tether is instrumented to provide measurements of the machine's three motions: vertical translation, forward translation, and rotation about the axis of the boom. [31] [32]



(a) Schematic representation of the JenaFox robot. (Adapted from [33]) (b) Definition of the associated coordinate system.

Figure 3.1: Schematic representation of the JenaFox bipedal walking robot (a) with its associated coordinate system (b). The bipedal robot consists of a torso connected to two segmented legs, each of which has an upper and a lower link. The abscissa axis (X-axis, orange) points in the direction of motion, the ordinate axis (Y-axis, green) points upward. The trunk of the robot is attached to a boom via a freely rotating joint which constrains the motion of the robot on a sphere. The planar motion is thus restricted to the sagittal plane (i.e. the plane spanned between the abscissa axis and ordinate axis).

The simulation of the JenaFox robot is created in MATLAB[®] Simulink R2022a as a Simscape multi-body model. The solver settings used for the simulation are listed in table 3.1.

Table 3.1: Solver settings for the MATLAB[®] Simulink simulation of the JenaFox robot.

Solver setting	Value
Solver type	variable-step
Solver	auto(ODE15s)
Max step size	0.1
Min step size	auto
Relative tolerance	0.01
Absolute tolerance	0.001

3.2 Neural Network Controller

In the simulation, a neural network controller based on the work of Geng, Porr, and Wörgötter [10] is used. The authors propose that a bio-inspired neural network controller may perform better in biped control than other comparable solution methods, such as zero moment point or inverted pendulum control, as it guarantees a stable gait even at high speeds. A neural network controller is a type of artificial intelligence algorithm that uses the principles of artificial neural networks to control the behavior of a system. Neural networks are modeled after the structure and function of the human brain, and they are trained using large amounts of data to learn how to perform a particular task. In the context of a neural network controller, the network is trained to produce control signals for a system based on inputs that represent the state of the system. These inputs could include sensor readings, past control signals, or other relevant information about the system. The neural network then outputs control signals that are used to regulate the behavior of the system. One of the key benefits of using a neural network controller is that, despite being highly scalable and flexible, it can learn to perform complex tasks that are difficult to describe mathematically. For example, a neural network controller could be trained to control a robot to walk, swim, or fly in a way that is similar to how animals perform these tasks. The network can learn from examples and adapt to new situations, making it well-suited for tasks that are subject to unpredictable variations or changing conditions. [10]

Despite its many benefits, there are also some challenges associated with using a neural network controller. One of these challenges is that it can be difficult to interpret how the network is making decisions, since the internal workings of the network are often highly complex and non-linear. Identifying and correcting errors in the network's behavior is therefore a demanding task. Another challenge is that neural networks are often trained using large amounts of data. The downside of this approach is its intensive and time-consuming computation. Therefore it is difficult to use neural network controllers in real-time applications, where the control signals need to be generated quickly and with a high level of accuracy. [10]

Table 3.2 gives an overview of the control scheme used for the JenaFox robot. Touchdown and reaching the anterior extreme angle (AEA) of either hip angle triggers the corresponding action. When the target is reached the power of the moving motors is switched off. Thus, the phases of the gait are:

1. Until the moment of touchdown, the right knee is extended while the right hip is flexed.
2. As soon as the double support phase is reached, the right hip begins to extend while the left knee flexes, thus leaving the ground. The double support phase is relatively short.
3. When the left knee is fully bent, the left hip begins to flex while the right hip continues to extend. The left leg thus surpasses the right and is now in front.
4. When the left hip reaches the AEA, the left knee begins to extend. The right hip remains extended.
5. Before touchdown, the right hip and the left knee are extended to their limits.

Table 3.2: Overview of the control scheme used for the JenaFox robot. Touchdown (TD) and reaching the anterior extreme angle (AEA) of either hip angle triggers the corresponding action. When the target is reached the power of the moving motors is switched off. In the images, the events are shown as dark stick figures and the corresponding actions as light stick figures. (Adapted from [32], p. 36)





Event	1. TD _r		2. HL@AEA		3. TD _l		4. HR@AEA	
	<i>action</i>	<i>goal</i>	<i>action</i>	<i>goal</i>	<i>action</i>	<i>goal</i>	<i>action</i>	<i>goal</i>
left hip (HL)	flex	AEA			extend	PEA		
left knee (KL)	flex	PEA	extend	AEA	hold	AEA		
right hip (HR)	extend	PEA				flex	AEA	
right knee (KR)	hold	AEA			flex	PEA	extend	AEA
								
	L R		R L		R L		L R	

Figure 3.2 shows the control parameters used for the joint angles according to the International Society of Biomechanics (ISB)¹ convention [34]. The parameter set consists of eight angles and five voltage values, i.e. for both the left and right leg two extreme angles each for hip and knee with respective voltage values for extension and flexion of each joint. The fifth voltage value represents the hold voltage of the knee in stance to keep the leg straight. [32]

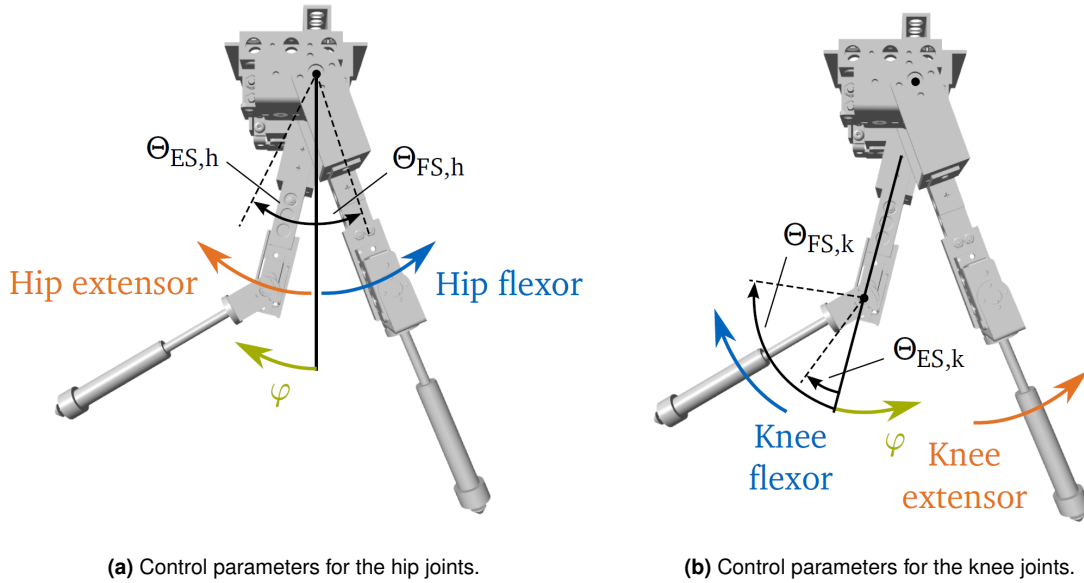


Figure 3.2: The control parameters for the hip (a) extensor $\theta_{ES,h}$ (orange) and flexor $\theta_{FS,h}$ (blue) as well as the knee (b) extensor $\theta_{ES,k}$ (orange) and flexor $\theta_{FS,k}$ (blue) joint angles according to the International Society of Biomechanics convention. (Adapted from [34])

The AEA is obtained by mapping the angle of the projected velocity vector, i.e. the velocity vector of the CoM \mathbf{v}_{CoM} projected down to the hip with a mapping function. The projected velocity vector \mathbf{v}_{CH} is calculated as the cross product of the angular velocity of the CoM $\dot{\phi}_{CoM}$ with the vector from the hip to the CoM summed with the translational velocity of the CoM:

¹The ISB is a non-profit organization founded in 1973 dedicated to promoting the study and application of biomechanics around the world.

$$\mathbf{v}_{CH} = \begin{bmatrix} \mathbf{v}_{CH_x} \\ \mathbf{v}_{CH_y} \\ 0 \end{bmatrix} = \begin{bmatrix} \mathbf{v}_{CoM_x} \\ \mathbf{v}_{CoM_y} \\ 0 \end{bmatrix} + \left(\begin{bmatrix} 0 \\ 0 \\ \dot{\phi}_{CoM} \end{bmatrix} \times \begin{bmatrix} x_{hip} - x_{CoM} \\ y_{hip} - y_{CoM} \\ 0 \end{bmatrix} \right). \quad (3.1)$$

The corresponding angle ρ is obtained by

$$\rho = \arctan2\left(\frac{\mathbf{v}_{CH_y}}{\mathbf{v}_{CH_x}}\right) \quad (3.2)$$

where $\arctan2$ is the four-quadrant inverse tangent, returning values in the closed interval $[-\pi, \pi]$, as shown in figure 3.3a. Note that ρ and the AEA are oriented in opposite directions, as shown in figure 3.3b.

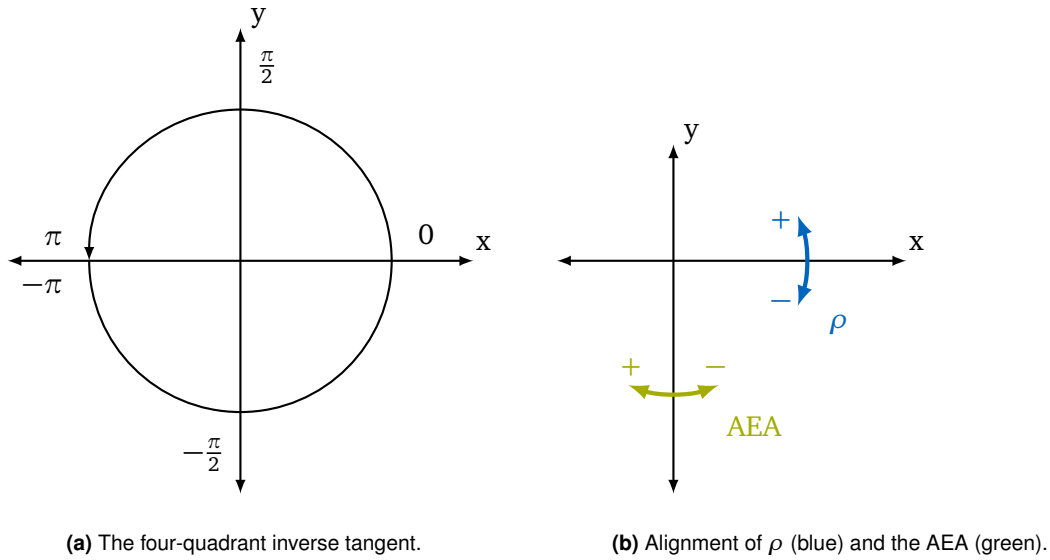


Figure 3.3: Graphical representation of the four-quadrant inverse tangent, returning values in the closed interval $[-\pi, \pi]$ (a) and alignment of ρ , the angle of the projected velocity vector \mathbf{v}_{CH} (blue), and the anterior extreme angle (AEA) (green). Note that the angles are oriented opposite to each other (b).

In order to achieve an adequate mapping from ρ to the AEA, various mapping functions were tested. The first set of experiments tested linear functions that set the AEA in direct proportional dependence to ρ , with the desired effect that the steeper ρ becomes, the steeper should also the AEA become to consequently obtain a steeper angle of attack α_{TD} and thus exchange as much vertical for horizontal velocity as possible. A selection of linear functions used is given in the following figure 3.4. However, it quickly became apparent that a linear mapping function is not optimal in many ways, since these tend to quickly leave the interval of reasonable values of the AEA. Thus, the next step was to try to achieve a better mapping via exponential functions, which are shown in figure 3.5. One problem with exponential mapping functions is that there only needs to be a very small change in ρ to cause a large change in the AEA. Thus, a sigmoid² function was used to map the values of ρ to obtain

²The sigmoid function is a mathematical function known for its characteristic "S"-shaped sigmoid curve and commonly used in machine learning and neural networks, where it can be used as a type of activation function that maps any real-valued number to a value between 0 and 1, which makes it useful for modeling probabilities and binary classification problems.

values of the AEA in a range between -10° and -25° . Mapping ρ with the following sigmoid function yields the AEA:

$$AEA = \frac{15}{1 + e^{k \cdot \rho + d}} - 25 \quad (3.3)$$

where k depicts a proportionality constant and d is an offset, i.e. a shift of the function along the abscissa axis. Values of $k = 0.2$ and $d = 4$ were chosen to map the values of ρ to obtain according values of the AEA in a range between -10° and -25° , as shown in figure 3.6. A summary of the control parameters is given in table 3.3 and table 3.4.

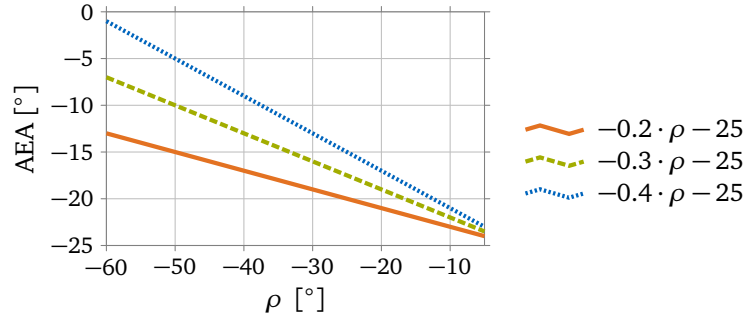


Figure 3.4: Linear mapping functions that set the anterior extreme angle (AEA) in direct proportional dependence to ρ .

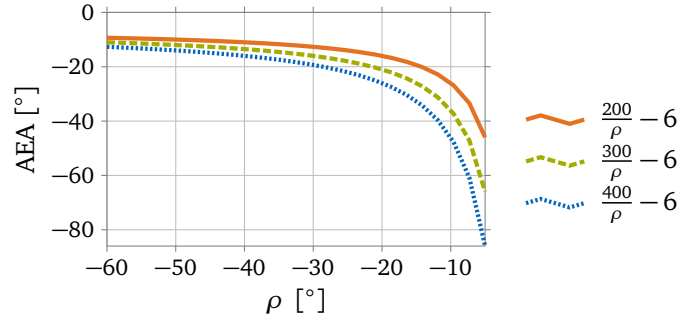


Figure 3.5: Exponential mapping functions that set the anterior extreme angle (AEA) in exponential dependence to ρ .

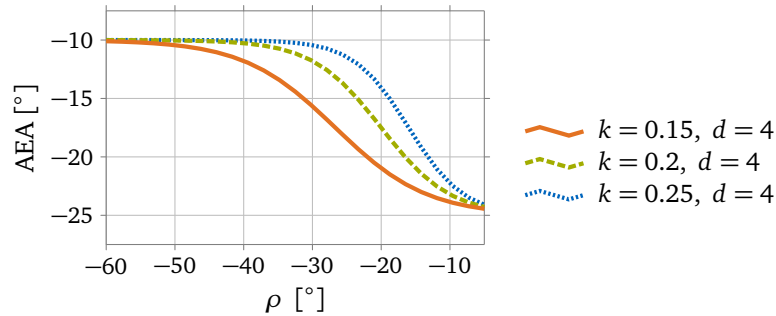


Figure 3.6: Sigmoid mapping functions and graphical representation of equation 3.3. The sigmoid function maps the projected velocity vector ρ to obtain the anterior extreme angle (AEA) in a range between -10° and -25° .

Table 3.3: Overview of the used control parameters for the sensory neurons, i.e. the joint angles of the hip extensor $\theta_{ES, h}$ and flexor $\theta_{FS, h}$ as well as the knee extensor $\theta_{ES, k}$ and flexor $\theta_{FS, k}$.

Control parameters for sensory neurons	Description	Value	Unit
$\theta_{ES, h}$	Threshold for hip extensor	5	[°]
$\theta_{FS, h}$	Threshold for hip flexor	AEA	[°]
$\theta_{ES, k}$	Threshold for knee extensor	-5 - -3	[°]
$\theta_{FS, k}$	Threshold for knee flexor	-80	[°]

Table 3.4: Overview of the used control parameters for the motor neurons. τ is a time constant associated with the passive properties of the cell membrane, M_{AMP} represents the magnitude of the servo amplifier. GM_h and GM_k depict the gain of the hip and knee motor, respectively.

Control parameters for motor neurons	Description	Value	Unit
τ	Time constant	0.01	[s]
M_{AMP}	Magnitude of the servo amplifier	3	—
GM_h	Gain of the hip motor	1.4 - 1.8	—
GM_k	Gain of the knee motor	$0.9 \cdot GM_h$	—

τ is a time constant associated with the passive properties of the cell membrane [9] and M_{AMP} represents the magnitude of the servo amplifier [10]. In the course of this work, the gain of the hip motor GM_h was modulated in the range between 1.4 and 1.8 in steps of 0.1. Furthermore, the threshold for the knee extensor $\theta_{ES, k}$ was modulated in the range between -5° and -3° in steps of 0.25. The best results were obtained with $GM_h = 1.6$ and $\theta_{ES, k} = -4.25^\circ$. The initial velocities of the CoM were set via the following equations:

$$\begin{aligned} v_{CoM_x, IC} &= |v_{CoM}| \cdot \cos(\lambda) \\ v_{CoM_y, IC} &= |v_{CoM}| \cdot \sin(\lambda) \end{aligned} \quad (3.4)$$

where $|v_{CoM}|$ is the magnitude and λ the angle of the velocity vector of the CoM.

3.3 Vertical Leg Orientation

The vertical leg orientation (VLO) refers to the orientation of the leg of a bipedal robot relative to the ground and is defined as the angle between the ordinate axis (perpendicular to the ground) and the line connecting the foot and hip joint of the robot. In a normal walking gait, the VLO changes throughout the stride cycle as the robot moves from one foot to the other. During the stance phase, the VLO starts at a relatively small angle, increases as the robot transfers weight over the stance leg, and reaches its maximum value just before the swing phase. During the swing phase, the VLO decreases as the swing leg moves forward, reaches its minimum value just before the footstrike, and then increases again as the swing leg moves into the stance phase. [36]

The JenaFox robot is capable of periodic gait patterns such as walking and running, where a gait pattern is fully described by the system parameters and initial conditions. In the course of this work, the initial conditions are chosen so that the stance leg is in contact with the ground and vertically oriented, i.e. the CoM is exactly above the foot point ($x_{CoM} = x_{FP_1}$), meaning that the horizontal position is zero with respect to the actual foot point. A single step is completed when the swing leg attains ground contact and the CoM is orthogonally above the second foot point ($x_{CoM} = x_{FP_2}$), as shown in figure 3.7. The simulation starts at the moment of vertical leg orientation during single support phase (VLO₀) and ends after one step is completed at VLO of the opposite leg (VLO₁). These initial conditions can be used to reduce the number of independent initial conditions. [36]

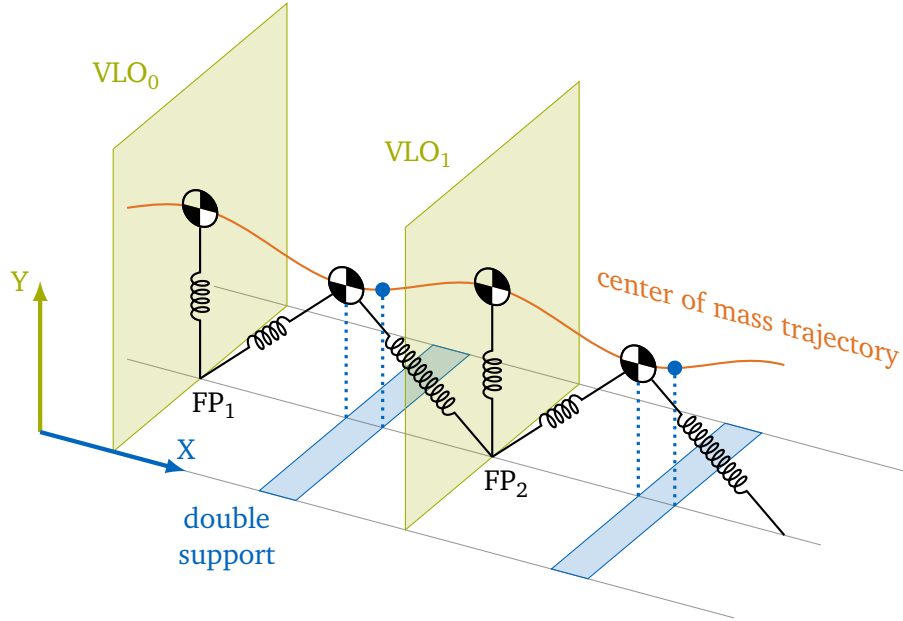


Figure 3.7: The bipedal spring mass model for walking. The simulation starts at the moment of vertical leg orientation (VLO) during single support phase (VLO₀, green) and ends after one step is completed at VLO of the opposite leg (VLO₁, green). The phase of the double support is shown in blue. The trajectory of the center of mass is drawn in orange. (Adapted from [36], p. 1)

3.4 Trajectory Optimization

Trajectory optimization is a method for designing the motion of a system to achieve a desired goal. It involves the calculation of an optimal path taking various constraints and objectives into account. The term trajectory refers to the path an agent travels as a function of time. The term trajectory optimization is therefore the set of methods used to obtain the best trajectory, usually by selecting appropriate inputs to the system, i.e. controls, as functions of time. The comprehensive policy of optimization is to minimize the objective function subject to a number of constraints and restrictions. [21] In the course of this work a trajectory optimization was performed via finding a minimum of constrained nonlinear multivariable functions.

The process typically involves the following steps [21]:

1. Modeling the robot's dynamics: A mathematical model of the robot's movement is created, which takes into account the robot's kinematics, dynamics, and control inputs.

2. Specifying the constraints: The constraints that must be satisfied by the robot's motion are defined, such as bounds on the joint angles and torques, as well as collision avoidance constraints.
3. Defining the objective: The objective function to be optimized is defined, which might include a trade-off between energy efficiency, speed, and smoothness of the motion.
4. Solving the optimization problem: An optimization algorithm is applied to find the path that minimizes the objective function while satisfying the constraints.
5. Generating the motion trajectory: The optimal path is transformed into a set of points that define the motion trajectory for the robot.

The following sections describe the individual steps that were carried out in more detail.

Assumptions

Within this work it is assumed that the trajectory is single-phase and of continuous time, meaning the system dynamics are continuous throughout the entire trajectory. The dynamics, the objective, and the constraints are smooth, consistent and potentially non-linear. Furthermore, the robot is considered to be left-right symmetric, allowing to search for a periodic walking gait with a single step instead of a stride. A periodic gait requires that the joint trajectories, consisting of the joint angles, their rates, and the associated torques, are the same for each successive step. [21]

Constraints

The first and possibly most important constraint is the system dynamics. In addition, limits are defined for the boundary condition, restricting the initial and final states of the system, including upper and lower limits for the joint angles and joint velocities. Furthermore, the initial state is limited to the VLO_0 , i.e. the stance leg always starts vertically.

Nonlinear Programming

Most direct collocation methods transform a continuous-time trajectory optimization problem into a nonlinear program (NLP), i.e. a constrained parameter optimization problem that has nonlinear terms in either its objective or its constraint function. This nonlinearity makes NLP problems more difficult to solve, as the objective function and/or constraints can have multiple local minima (or maxima) and the global minimum (or maximum) may not be easily accessible. [21] A common formulation for a nonlinear program is as follows:

$$\begin{aligned}
 &\min_{\mathbf{a}} && f(\mathbf{a}) \\
 &\text{subject to} && h(\mathbf{a}) = 0 \\
 & && g(\mathbf{a}) \leq 0, \\
 & && \mathbf{a}_{lb} \leq \mathbf{a} \leq \mathbf{a}_{ub}
 \end{aligned} \tag{3.5}$$

where \mathbf{a} denotes the vector of design variables, $f(\mathbf{a})$ the objective function, $h(\mathbf{a})$ the equality constraint functions, $g(\mathbf{a})$ the inequality constraint functions and \mathbf{a}_{lb} , \mathbf{a}_{ub} the lower and upper bounds, respectively.

System Dynamics

During single support (see figure 3.7), the system has six degrees of freedom (DoF): the absolute angles of both lower legs, i.e. of the knee joints (q_5 and q_7), both upper legs, i.e. of the hip joints (q_4 and q_6), the torso (q_3) as well as the vertical displacement, which depends on the springs mounted inline to the legs (q_2). The DoF can be seen in figure 3.8. Hereafter, the DoF of the system are cumulated into the single vector \mathbf{q} . Since it is a second order dynamical system, the derivative of the configuration, $\dot{\mathbf{q}}$ must also be included. Thus, the state can be described with $[\mathbf{q} \ \dot{\mathbf{q}}]^T$ and the dynamics as $[\dot{\mathbf{q}} \ \ddot{\mathbf{q}}]^T$, where \mathbf{q} are the angles, $\dot{\mathbf{q}}$ the angular rates and $\ddot{\mathbf{q}}$ the accelerations, respectively. Since the initial and final states of the optimization problem are defined using the VLO, the start and end position of the stance leg is always vertically. Thus, the respective hip and knee angles as well as the corresponding angular velocities can be neglected. This results in six parameters which have to be considered: The hip and knee angles of the swing leg, the angle of the upper body and their angular velocities. Furthermore, to obtain a variation of the velocity vector, λ , i.e. the angle of \mathbf{v}_{CoM} , is also included. Table 3.5 shows the initial condition used in the multi-body simulation.

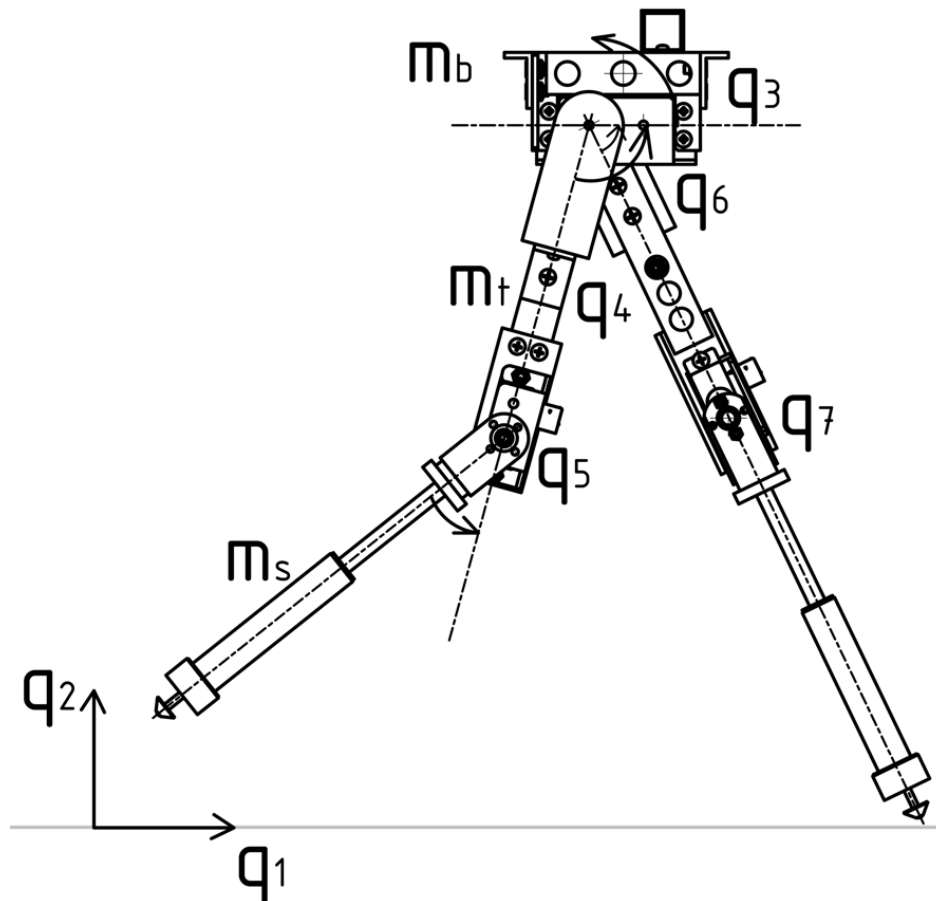


Figure 3.8: Degrees of freedom of the basic mechanical setup. The trunk (mass m_b) has three degrees of freedom (q_1 , q_2 , q_3), hip and knee of the right leg connect the thigh (m_t) to the body and shank (m_s) to the thigh respectively by one degree of freedom each (q_4 , q_5), the same counts for the left side (q_6 , q_7). (Adapted from [32], p. 37)

Table 3.5: Initial conditions used in the multi-body simulation consisting of the knee and hip angles of the swing leg, $q_{5, IC}$ and $q_{4, IC}$, the angle of the torso $q_{3, IC}$ as well as their corresponding velocities $\dot{q}_{5, IC}$, $\dot{q}_{4, IC}$ and $\dot{q}_{3, IC}$. In addition, λ_{IC} , i.e. the initial angle of \mathbf{v}_{CoM} , was passed to the optimizer.

Initial conditions	Description	Value	Unit
$q_{5, IC}$	Angle of the right knee	-29	[°]
$q_{4, IC}$	Angle of the right hip	-15	[°]
$q_{3, IC}$	Angle of the torso	15	[°]
λ_{IC}	Angle of \mathbf{v}_{CoM}	10	[°]
$\dot{q}_{5, IC}$	Angular velocity of the right knee	0	$\left[\frac{\text{rad}}{\text{s}}\right]$
$\dot{q}_{4, IC}$	Angular velocity of the right hip	0	$\left[\frac{\text{rad}}{\text{s}}\right]$
$\dot{q}_{3, IC}$	Angular velocity of the torso	0	$\left[\frac{\text{rad}}{\text{s}}\right]$

The used upper and lower bounds which were passed to the optimizer can be found in appendix A. The lower bounds are specifies as

$$\begin{aligned}
 q_{i, IC} &\geq q_{i, lb} \quad \forall i, \\
 \dot{q}_{i, IC} &\geq \dot{q}_{i, lb} \quad \forall i, \\
 \lambda_{IC} &\geq \lambda_{lb},
 \end{aligned} \tag{3.6}$$

the upper bounds are specifies as

$$\begin{aligned}
 q_{i, IC} &\leq q_{i, ub} \quad \forall i, \\
 \dot{q}_{i, IC} &\leq \dot{q}_{i, ub} \quad \forall i, \\
 \lambda_{IC} &\leq \lambda_{ub},
 \end{aligned} \tag{3.7}$$

where $q_{i, IC}$ and $\dot{q}_{i, IC}$ depict the initial conditions of each joint i and λ_{IC} the initial angle of \mathbf{v}_{CoM} .

Objective Function

To ensure that the walking gait is periodic, the sum of absolute deviations between the initial and final state is used as the cost function. The states consist of \mathbf{q} and $\dot{\mathbf{q}}$, with the absolute value of the torso angle to allow the frequency of the torso to be potentially half the frequency of a full step

$$f = \sum_{i=3}^7 |q_i(t_{end}) - q_i(t_0)| + |\dot{q}_i(t_{end}) - \dot{q}_i(t_0)| \tag{3.8}$$

where $t_0 = 0$ represents the initial state (i.e. VLO_0) and t_{end} represents the final state (i.e. VLO_1). Further, the knee angle of the swing leg at touchdown $q_{5, TD}$ is included with an exponential penalty of the form

$$y = -20 \cdot (0.6^{|x|} - 1) \tag{3.9}$$

which converges to a penalty value of 20, as can be seen in the following figure 3.9. Note that the knee is fully extended at $q_{5, TD} = 0^\circ$. This ensures the smallest possible knee angle and thus the most extended leg possible at touchdown.

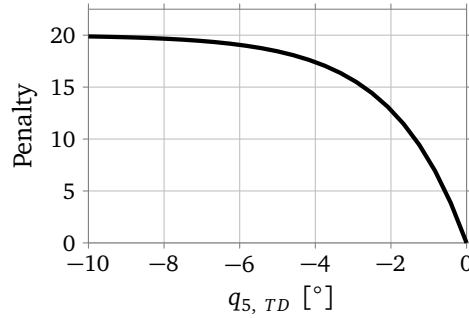


Figure 3.9: Exponential penalty of the knee angle of the swing leg at touchdown $q_{5, TD}$. Note that the knee is fully extended at $q_{5, TD} = 0^\circ$. The penalty converges to a value of 20.

The same penalty was also applied to the final state of the hip and knee angles of the stance leg, to keep the angles as small as possible and thus to regain the upcoming VLO_1 to the greatest possible extent again. Choosing an appropriate cost function is desirable to obtain smooth, well-behaved solutions and to ensure good convergence of the NLP. Among others, the CoT is a widely used objective function, which, however, is difficult to optimize because the solutions tend to have discontinuities. [21]

Termination conditions

To increase the robustness of the model, possible error modes are identified in which the model shows unexpected or undesired behavior. The identified conditions are presented in table 3.6, such as the CoM or one of the knees falling below a threshold in height, the robot starting to walk backwards as well as reaching a time or distance limit. If any of these cases occur, the simulation is aborted and the cost is penalized with a penalty function similar to the one used for the angles (see equation 3.9).

Table 3.6: Identified failure modes of the system which may occur. A total of six failure modes were identified, the center of mass (CoM) or one of the knees falling below a threshold in height, the robot starting to walk backwards as well as reaching a time or distance limit. If any of these cases occur, the simulation is aborted and the cost is penalized with a penalty function.

Failure Mode	Condition
Falling	$y_{CoM} \leq 0.15 \text{ m}$
Knee falling	$y_{knee_r}, y_{knee_l} \leq 0.028 \text{ m}$
Walking backwards	$v_{CoM_x} \leq -1 \frac{\text{m}}{\text{s}}$
Time limit	$t_{end} \geq 3.0 \text{ s}$
Distance limit	$x_{CoM} \geq 0.5 \text{ m}$

3.5 Summary

In this chapter the individual steps, which are necessary to design a controller for the torso stabilization of a bipedal robot, are considered in detail. A MATLAB® Simulink implementation of the JenaFox model was provided. The used neural network controller is based on the work of Geng, Porr, and Wörgötter [10]. The initial and final conditions are defined by the vertical leg orientation (VLO). In order to be able to evaluate the individual iterations, a trajectory optimization problem was formulated in which the best solution is also the most periodic one, i.e. the solution in which the difference between the initial state (VLO_0) and final state (VLO_1) is as small as possible. Furthermore, termination conditions were identified to avoid undesired behavior.

Chapter 4

Evaluation

The overall goal of this project is to obtain a control law via reverse engineering the model dynamics to answer the following question: How must the AEA be set in relation to ρ to get a touchdown with the current state $[\mathbf{q} \quad \dot{\mathbf{q}}]^T$ so that the periodicity of the gait is preserved in the subsequent step? By simulating and analyzing the dynamics of the entire system, an attempt is made to deduce a control law. The ideal case would be to find a constant offset which, independent of the magnitude of the velocity vector \mathbf{v}_{CH} , always leads to a periodic solution.

To find an answer to this question, the optimizer was left to find a solution as periodic as possible via the cost function from equation 3.8. A preliminary sweep in a feasible range was performed considering GM_h and $\theta_{ES, k}$ separately, in order to observe a tendency of their influence in the behavior of the system. Note that varying $\theta_{ES, k}$ does not increase the velocity significantly, however, increasing the gain of the hip motor GM_h does, since this straightly affects the output voltage of the motors, but the system also becomes increasingly unstable, to the point where it is not able to walk anymore. $\theta_{FS, k}$ was excluded from the sweep as it seems to have a much more erratic behavior. Additionally, since any deviation from $\theta_{ES, h}$ seemed to negatively affect the robustness of the system, this parameter was left at the default value of 5.

Finding appropriate initial parameters for a stable gait is one of the biggest challenges in modelling a spring-mass biped, which often turns out to be time-consuming and tedious. As it is not possible to analytically deduce the dependence of the stability of the system on the initial parameters, most of them have to be found through experiments. In addition, even small disturbances of the permissible parameters can quickly lead to instability of the entire system. In this project, most of the parameters were chosen according to appropriate experimental data from Geng et al. [10] and the remaining ones were determined by sweeping within a reasonable range. The parameters obtained from the sweep consist of

$$\begin{cases} \theta_{ES, k} = -4.25 \\ \theta_{FS, h} = \text{AEA} = \frac{15}{1+e^{0.2 \cdot \rho + 4}} - 25 \\ GM_h = 1.6 \end{cases} \quad (4.1)$$

The resulting walking gait using the parameters from equation 4.1 is summarized in table 4.1. The results of the performed MCA are summarized in table 4.2.

Table 4.1: The results of the walking gait.

Symbol	Description	Value	Unit
$x_{CoM, end}$	Distance covered	15	[m]
t_{end}	Time required	18.8502	[s]
\overline{v}_{CoM_x}	Average forward velocity	0.8379	$\left[\frac{m}{s}\right]$
$v_{CoM_x, max}$	Maximum instantaneous velocity	1.7803	$\left[\frac{m}{s}\right]$
$v_{CoM_x, min}$	Minimum instantaneous velocity	-0.7106	$\left[\frac{m}{s}\right]$
$y_{CoM, max}$	Highest vertical displacement	0.2907	[m]
$y_{CoM, min}$	Lowest vertical displacement	0.2031	[m]

Table 4.2: The results of the mechanical cost analysis.

Symbol	Description	Value	Unit
Fr	Froude number	0.2468	-
\sqrt{Fr}	Dimensionless velocity	0.4986	-
Θ	Average force angle	0.7285	[rad]
Λ	Average velocity angle	0.3704	[rad]
Φ	Average collision angle	0.9855	[rad]
CoT_{mech}	Mechanical Cost of Transport	0.5226	$\left[\frac{J}{mN}\right]$
κ	Collision fraction	0.8968	-

Compared to mammals from the literature, the CoT_{mech} of the robot is relatively high. Humans, for example, walk with $CoT_{mech} \approx 0.08$ and run with $CoT_{mech} \approx 0.28$ [25]. Figure 4.1 shows Θ , Λ and Φ as a fraction of their sum in a ternary diagram. The filled circles indicate bipedal gaits and the filled squares indicate quadrupedal gaits. The color of the symbols indicate the collision fraction κ with red indicating $\kappa = 1$ and purple $\kappa = 0$ (for spectrum of intermediate colors, see color scale at right). [25]

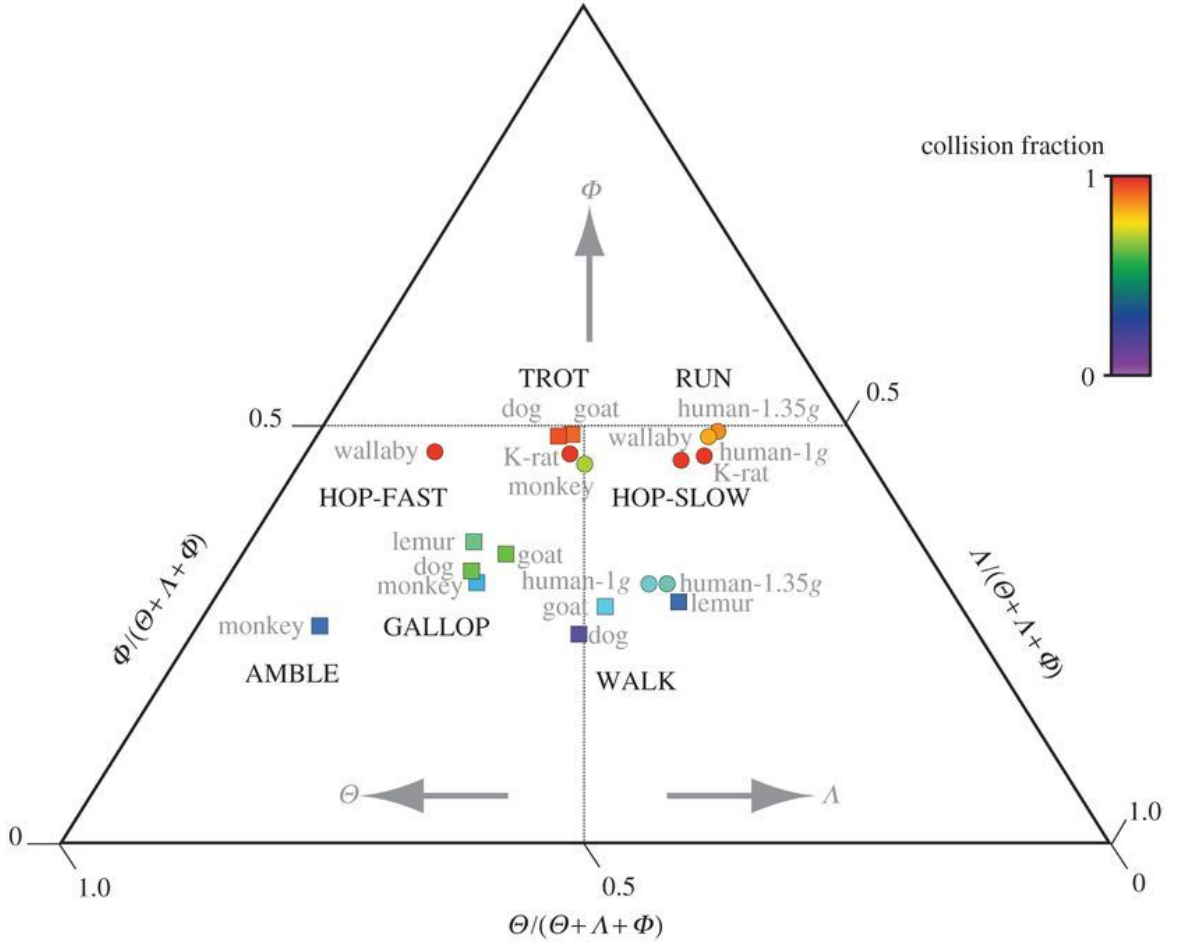
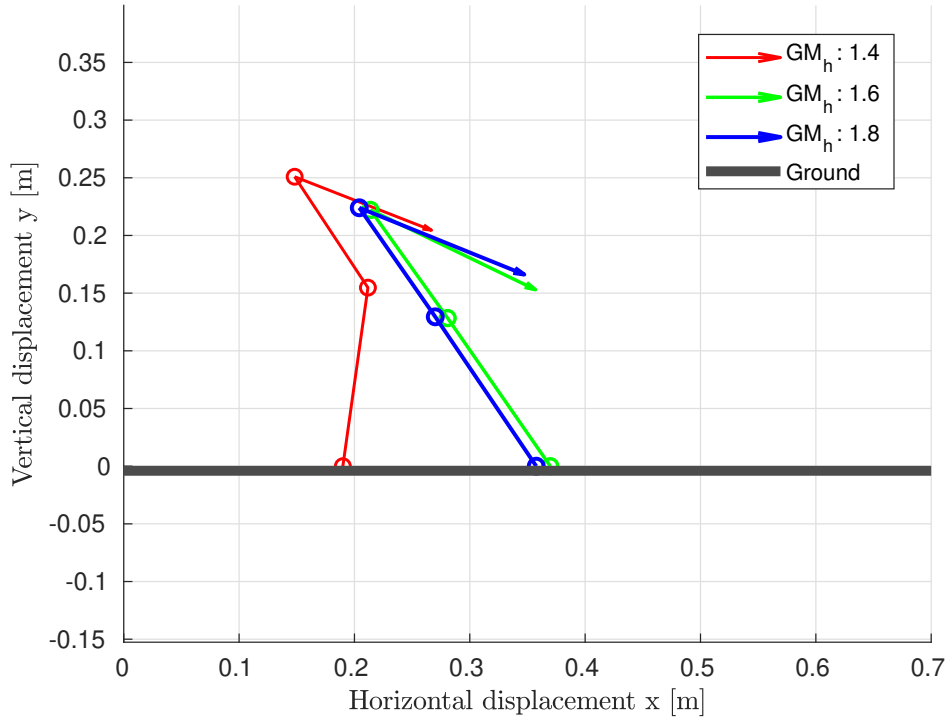
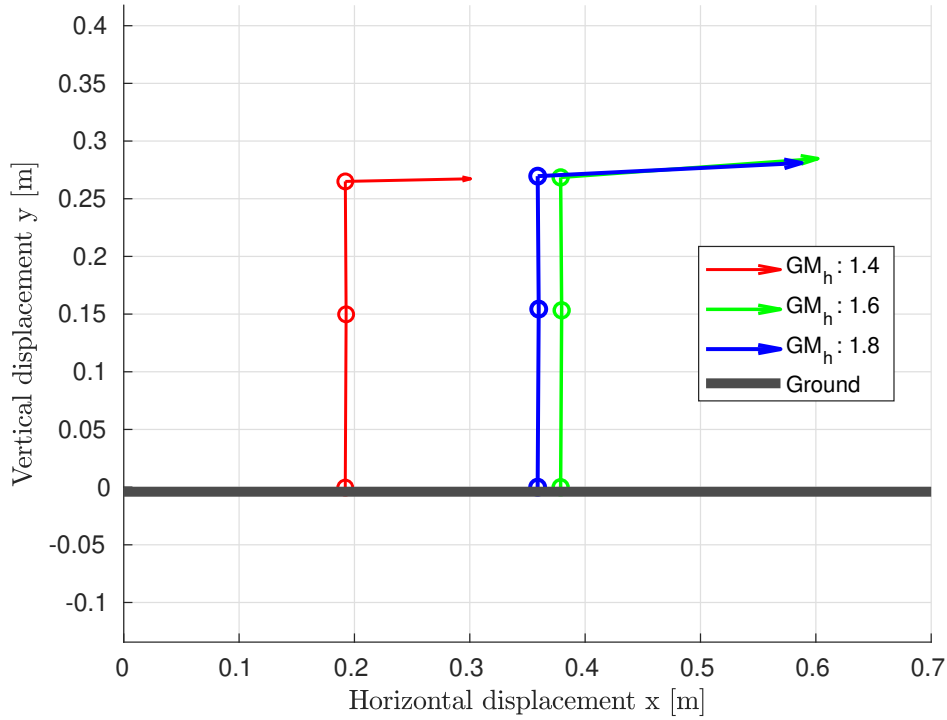


Figure 4.1: The collision-based analysis of selected mammals from the literature. Θ , Λ and Φ are shown as a fraction of their sum in a ternary diagram. The filled circles indicate bipedal gaits and the filled squares indicate quadrupedal gaits. The color of the symbols indicate the collision fraction κ with red indicating $\kappa = 1$ and purple $\kappa = 0$ (for spectrum of intermediate colors, see color scale at right). (Adapted from [25], p. 6)

Figure 4.2 shows the velocity vectors \mathbf{v}_{CoM} at touchdown (a) and at VLO_1 (b). At the beginning of the velocity vectors the leg position is shown schematically, where the hip, knee and ankle joints are drawn as circles. Accordingly, it can be seen that the robot performs the touchdown with a fully extended knee if $GM_h \geq 1.6$. With a GM_h of 1.4, the swing leg of the robot is not fast enough to reach an extended knee at touchdown. The velocity vectors at touchdown are always in the fourth quadrant, which means that the robot has a positive horizontal forward velocity ($\mathbf{v}_{CoM_x} > 0 \frac{m}{s}$) and a negative vertical velocity ($\mathbf{v}_{CoM_y} < 0 \frac{m}{s}$), in other words, the torso falls forward and is caught by the swing leg at touchdown. The velocity vectors at VLO_1 are always in the first quadrant, which means that the robot has a positive horizontal as well as vertical velocity ($\mathbf{v}_{CoM_x} \wedge \mathbf{v}_{CoM_y} > 0 \frac{m}{s}$). A single step is completed when the swing leg attains ground contact and the CoM is orthogonally above the second foot point ($x_{CoM} = x_{FP_2}$). The colors refer to the different motor gains, with red representing the lowest with $GM_h = 1.4$, and blue the highest with $GM_h = 1.8$. The angle of the velocity vector tends to get steeper the larger the motor gain GM_h , i.e. the faster the robot runs. A steeper velocity vector has more vertical than horizontal velocity and thus leads to a steeper angle of attack α_{TD} .



(a) The velocity vectors at touchdown. From this it can be seen that the robot performs the touchdown with a fully extended knee if $GM_h \geq 1.6$, as the three circles representing the joints form a straight line.



(b) The velocity vectors at VLO_1 , i.e. after a single step is completed, the swing leg attains ground contact and the CoM is orthogonally above the second foot point ($x_{CoM} = x_{FP_2}$).

Figure 4.2: Velocity vectors at touchdown (a) and at VLO_1 (b). At the beginning of the velocity vectors the leg position is shown schematically, where the hip, knee and ankle joints are drawn as circles. The colors refer to the different motor gains, with red representing the lowest with a GM_h of 1.4, and blue the highest with a GM_h of 1.8. The velocity vectors are scaled by a factor of 0.15.

Figure 4.3 shows the trajectory of the horizontal velocity of the CoM during the motion. For legibility purposes, the first 10 s of movement are displayed. The robot moves with an average forward velocity of $0.8379 \frac{m}{s}$. The amplitude of the horizontal velocity ranges from a maximum of $1.7803 \frac{m}{s}$ to a minimum of $-0.7106 \frac{m}{s}$. In order to minimize the energy consumption of the system, the amplitude deflection should be reduced and negative forward velocities avoided. The trajectory of the vertical velocity of the center of mass during the motion of the robot is shown in appendix B.

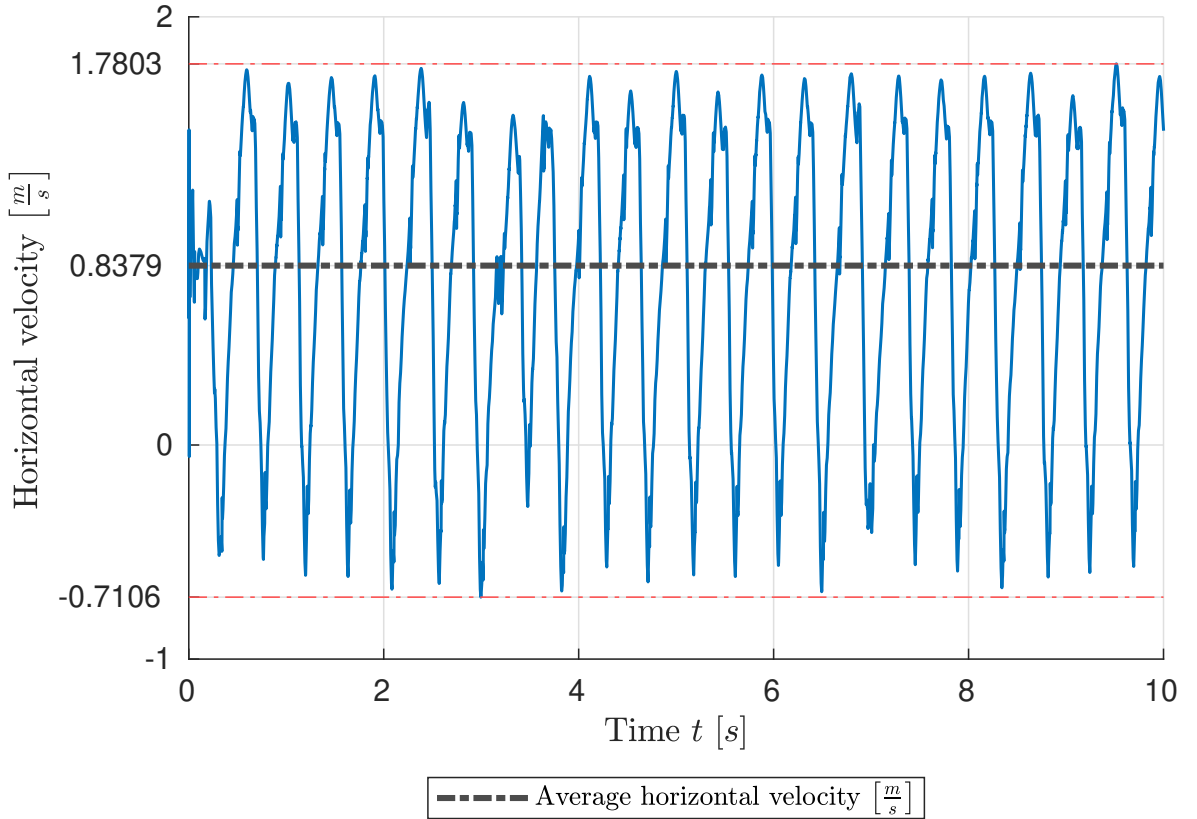


Figure 4.3: The trajectory of the horizontal velocity of the center of mass during the motion. For legibility purposes, the first 10 s of movement are displayed. The robot moves with an average forward velocity of $0.8379 \frac{m}{s}$. The amplitude of the horizontal velocity ranges from a maximum of $1.7803 \frac{m}{s}$ to a minimum of $-0.7106 \frac{m}{s}$.

Figure 4.4 shows the angle of the torso (q_3) and the right hip (q_4) with respect to the world from VLO_0 to VLO_1 . The phase of the double support is drawn in blue, the time of the touchdown is in the phase change of the single to the double support and is marked by the dashed line (blue). The torso makes a change of direction at the time of the touchdown, i.e. before the touchdown it falls forwards, while falling backwards again after the touchdown. One cycle of the gait of the JenaFox robot can be seen in figure 4.5, which starts at the moment of VLO_0 (a) and ends after one step is completed at VLO_1 of the opposite leg (h).

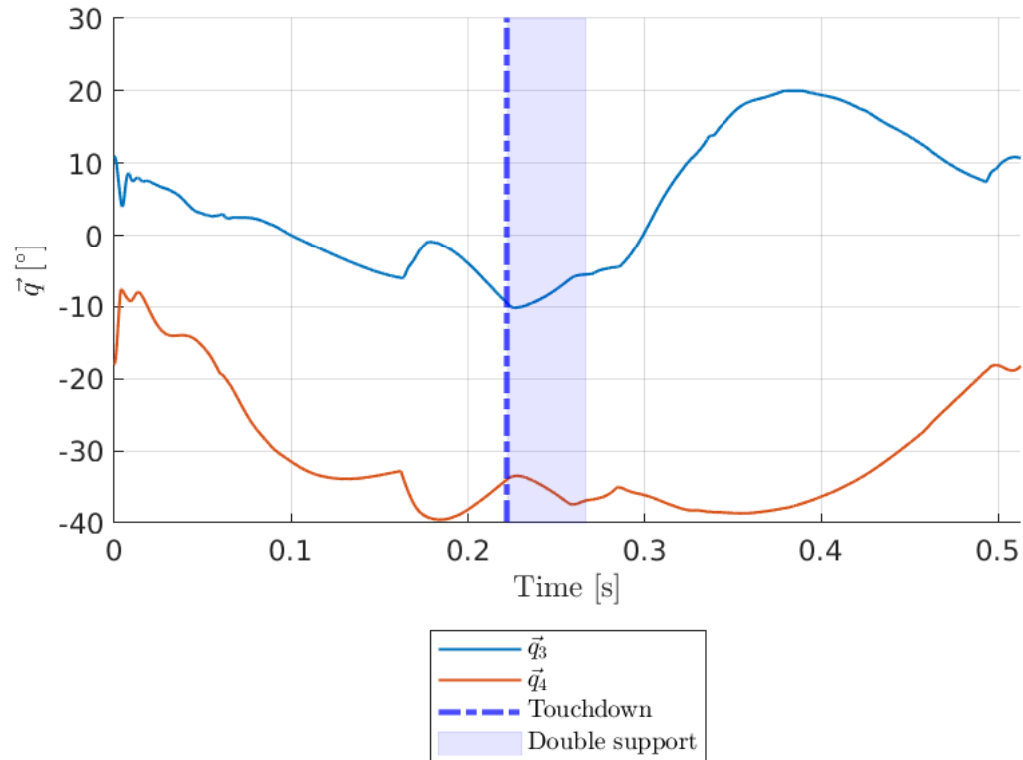


Figure 4.4: The angle of the torso (q_3) and the right hip (q_4) with respect to the world from VLO_0 to VLO_1 . The phase of the double support is drawn in blue, the time of the touchdown is in the phase change of the single to the double support and is marked by the dashed line (blue). The torso makes a change of direction at the time of the touchdown, i.e. before the touchdown it falls forwards, while falling backwards again after the touchdown.

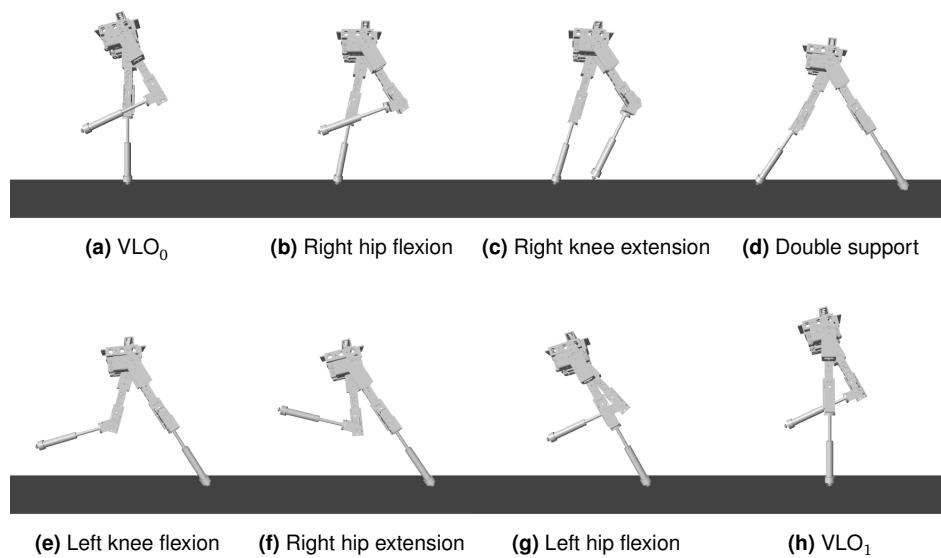


Figure 4.5: One cycle of the gait of the JenaFox robot, starting at the moment of VLO_0 (a) and ending after one step is completed at VLO_1 of the opposite leg (h).

4.1 Stability Analysis

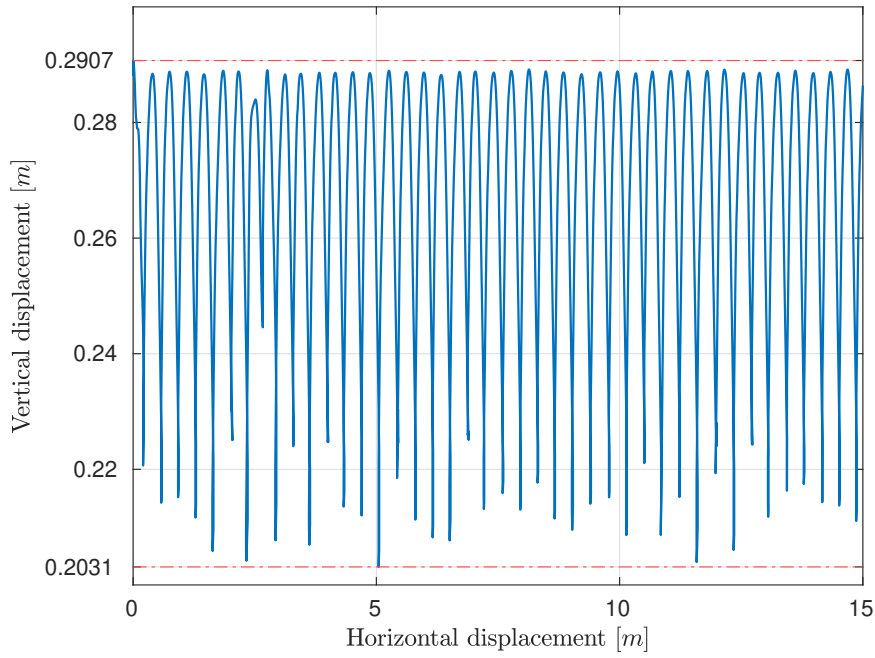
A first indicator of the stability of a walking system is the maximum displacement on the ordinate axis, as bigger oscillations tend to be related with poor robustness of the stability of the gait. Figure 4.6 shows the trajectory of the CoM, with the help of which a first impression of the stability can be gained, as the CoM remains between y_{min} and y_{max} at every instant. Note that the vertical displacement remains relatively continuous at the upper end, while strong oscillations occur at the lower end. In figure 4.6b a section of the vertical displacement is shown, where it can be seen that the robot reaches a negative horizontal displacement at the lower end, causing a loop. This is far from an ideal gait and is extremely energy consuming.

A quantitative analysis of the stability of the system can be achieved by evaluating the phase diagram¹. In a phase plot, each point in the phase space represents a unique state of the system, defined by the values of its state variables. If during each step the trajectory of the system in the phase plot tends to the limit cycle², the system is stable, i.e. the system will converge to the limit cycle regardless of the initial conditions, and the limit cycle will persist indefinitely. In an unstable limit cycle, on the other hand, the trajectory will approach the limit cycle for some initial conditions, but it will diverge from it for others. The existence of a limit cycle in the phase plot thus ensures (marginal) stability. [13] Figure 4.7 shows the phase plot of the simulation, i.e. the graphical representation of the behavior of the dynamical system in the phase space³. The plot shows the position of the torso of the JenaFox robot on the sagittal plane (i.e. the plane spanned between the abscissa axis (X-axis, orange) and ordinate axis (Y-axis, green), see figure 3.1b) during its motion and reveals that the robot is asymptotically stable in its gait. The simulation was stopped as soon as the robot reached a distance of 15 m. The vertical displacement of the torso in [m] is plotted on the abscissa axis, the vertical velocity in $\left[\frac{m}{s}\right]$ on the ordinate axis, respectively.

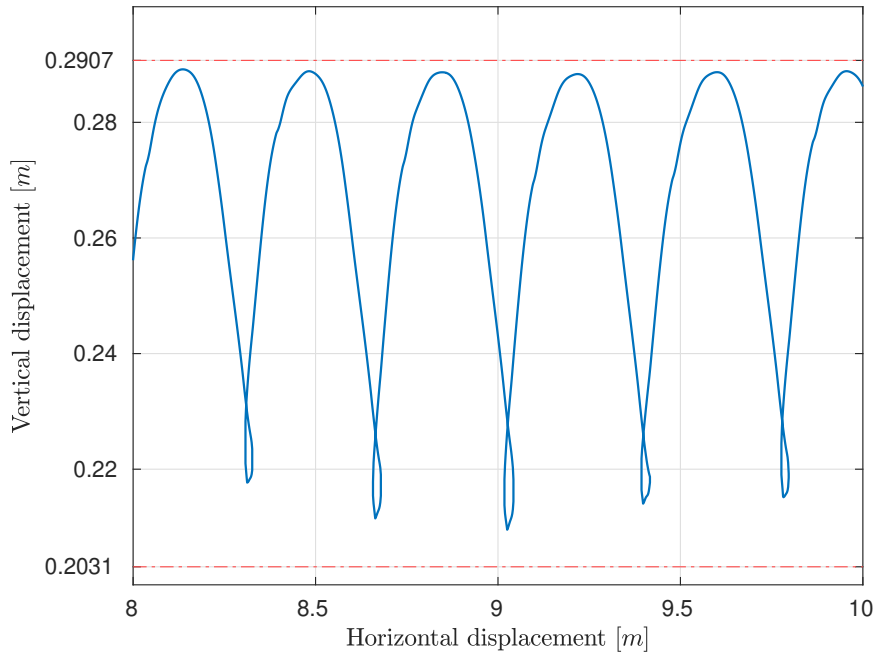
¹A phase diagram typically consists of a set of curves or trajectories that represent the time evolution of the system's state. Each trajectory represents the path that the system would follow in the phase space for a particular set of initial conditions. By plotting multiple trajectories with different initial conditions, it is possible to visualize the range of possible behaviors of the system. [13]

²The limit cycle is a type of behavior exhibited by some dynamical systems, in which the system oscillates or repeats its behavior indefinitely, but without necessarily converging to a steady state or equilibrium [13].

³The phase space refers to the set of all possible states of a system.

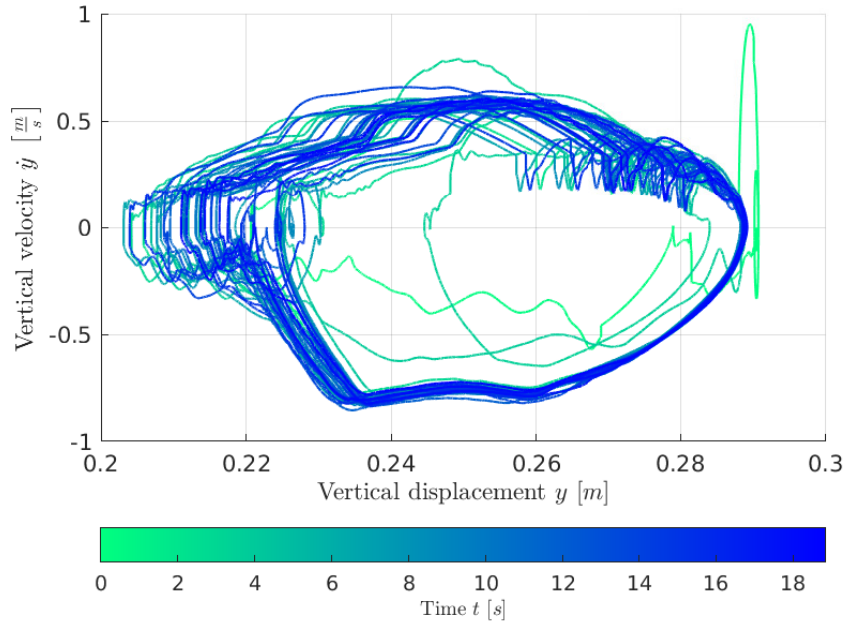


(a) The full trajectory of the CoM over the course of 15 m. Note that the vertical displacement remains relatively continuous at the upper end, while strong oscillations occur at the lower end.

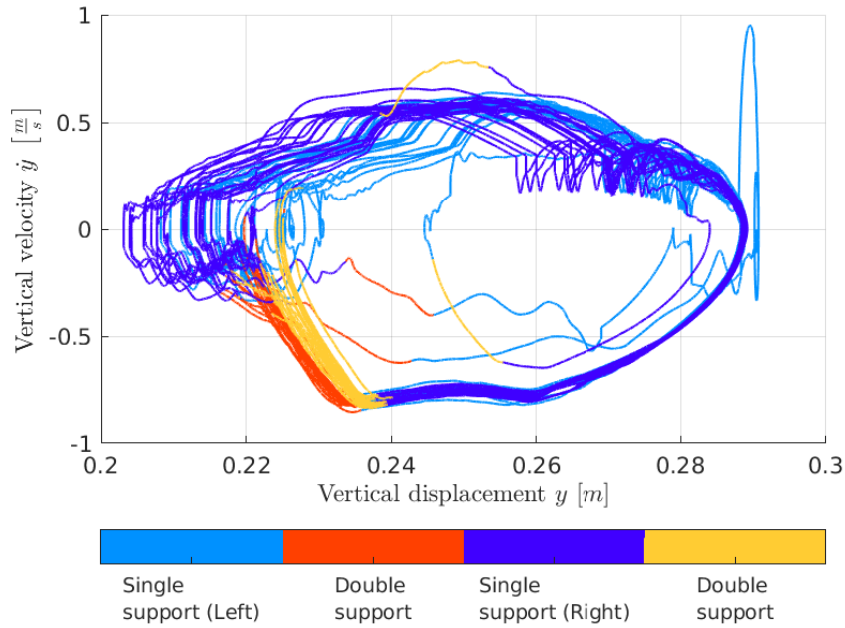


(b) A section of the CoM trajectory is shown, where it can be seen that the robot reaches a negative horizontal displacement at the lower end, causing a loop. This is far from an ideal gait and is extremely energy consuming.

Figure 4.6: The trajectory of the center of mass (CoM), with the help of which a first impression of the stability can be gained, as bigger oscillations tend to be related with poor robustness of the stability of the gait. The simulation was stopped after a distance of 15 m was reached (a). A more detailed section of the trajectory reveals a negative horizontal displacement at the lower end (b). The horizontal displacement of the torso in [m] is plotted on the abscissa axis, the vertical displacement in [m] on the ordinate axis, respectively.



(a) The phase plot of the simulation. The simulation was stopped after a distance of 15 m was reached. Time is represented by a colormap, which shows that the robot converges to an asymptotically stable gait with few oscillations.



(b) The phase plot of the simulation. The simulation was stopped after a distance of 15 m was reached. The ground state of the system is represented by a colormap, showing the two single support phases (light blue, dark blue) and the two double support phases (red, yellow).

Figure 4.7: The phase plot of the simulation, i.e. the graphical representation of the behavior of the dynamical system in the phase space over the entire simulation with color-encoded time (a) and ground state (b). The plot shows the position of the torso of the JenaFox robot on the sagittal plane during its motion and reveals that the robot is asymptotically stable in its gait. The vertical displacement of the torso in $[m]$ is plotted on the abscissa axis, the vertical velocity in $[\frac{m}{s}]$ on the ordinate axis, respectively.

4.2 Summary

This chapter presents the results and evaluates the implemented controller with quantitative parameters based on the mechanical cost analysis. In the course of this work, most of the parameters were chosen according to appropriate experimental data from Geng et al. [10] and the remaining ones were determined by sweeping within a reasonable range. The phase plot reveals that the robot is asymptotically stable in its gait. Compared to mammals from the literature, the CoT_{mech} of the robot is relatively high [25]. Although a periodic gait has been found, it is not energy efficient. Studying the velocities, it can be seen that the amplitude deflection of the horizontal velocity is quite large and even becomes negative - resulting in a negative horizontal displacement of the robot with a consequently high energy consumption, which should be addressed in further work.

Chapter 5

Conclusion and future work

By simulating and analyzing the dynamics of the entire system a control law was deduced, that sets the AEA in relation to ρ in a way that the periodicity of the gait is preserved in the subsequent step. Over trajectory optimization, choosing parameters according to appropriate experimental data and sweeping within a reasonable range, a set of parameters, which lead to an asymptotically stable gait, could have been found.

The presented optimizer used to tune the gait could even be the starting point to develop new promising gaits. A first step could be to generate a basin of attraction to analyze the error distance of the solution to the most periodic solution. Another future improvement could be an iterative optimization by taking the gait learned here, which is valid but not energy efficient, as the basis for another optimization procedure and to further refine the desired gait with additional penalty functions and constraints. Furthermore, the trajectory optimization could be extended by a Hermit-Simpson collocation, which is a numerical method for solving ordinary differential equations (ODEs) by approximating the solution using piecewise polynomials, based on two well-known numerical methods: the Hermite interpolation and the Simpson's rule for integration. The method is particularly useful for solving stiff ODEs with widely varying time scales, as it can handle rapid changes in the solution without requiring a high temporal resolution. [21]

An ongoing issue that should be addressed in further work is the extreme oscillations of the horizontal velocity (see figure 4.6a), which also include a negative horizontal displacement of the robot (see figure 4.6b). This results in an enormous energy demand, as the robot permanently accelerates and then decelerates again with the given gait. A possible solution approach would be to give the optimizer stricter constraints, for example, that the robot is not allowed to reach negative horizontal velocities at all ($v_{CoM_x} > 0 \frac{m}{s} \forall t$). However, at the current time of writing, no reasonable gait could have been found that takes stricter constraints into account. Finally, further objective functions can be tried, to ensure good convergence of the NLP. Among others, the CoT is a widely used objective function, which, however, is difficult to optimize because the solutions tend to have discontinuities. [21]

Appendix A

Upper and lower bounds of the design variables

Table A.1: Upper and lower bounds used in the optimization problem consisting of the initial conditions for the knee and hip angles of the swing leg, $q_{5, IC}$ and $q_{4, IC}$, the angle of the torso $q_{3, IC}$, their corresponding velocities $\dot{q}_{5, IC}$, $\dot{q}_{4, IC}$ and $\dot{q}_{3, IC}$ as well as λ_{IC} , the initial angle of \mathbf{v}_{CoM} .

Symbol	Description	Lower bound	Upper bound	Unit
$q_{5, IC}$	Angle of the right knee	-110	-10	$[\circ]$
$q_{4, IC}$	Angle of the right hip	-70	70	$[\circ]$
$q_{3, IC}$	Angle of the torso	-20	20	$[\circ]$
λ_{IC}	Angle of \mathbf{v}_{CoM}	-30	30	$[\circ]$
$\dot{q}_{5, IC}$	Angular velocity of the right knee	-3	3	$\left[\frac{\text{rad}}{\text{s}}\right]$
$\dot{q}_{4, IC}$	Angular velocity of the right hip	-3	3	$\left[\frac{\text{rad}}{\text{s}}\right]$
$\dot{q}_{3, IC}$	Angular velocity of the torso	-3	3	$\left[\frac{\text{rad}}{\text{s}}\right]$

Appendix B

Vertical velocity of the center of mass

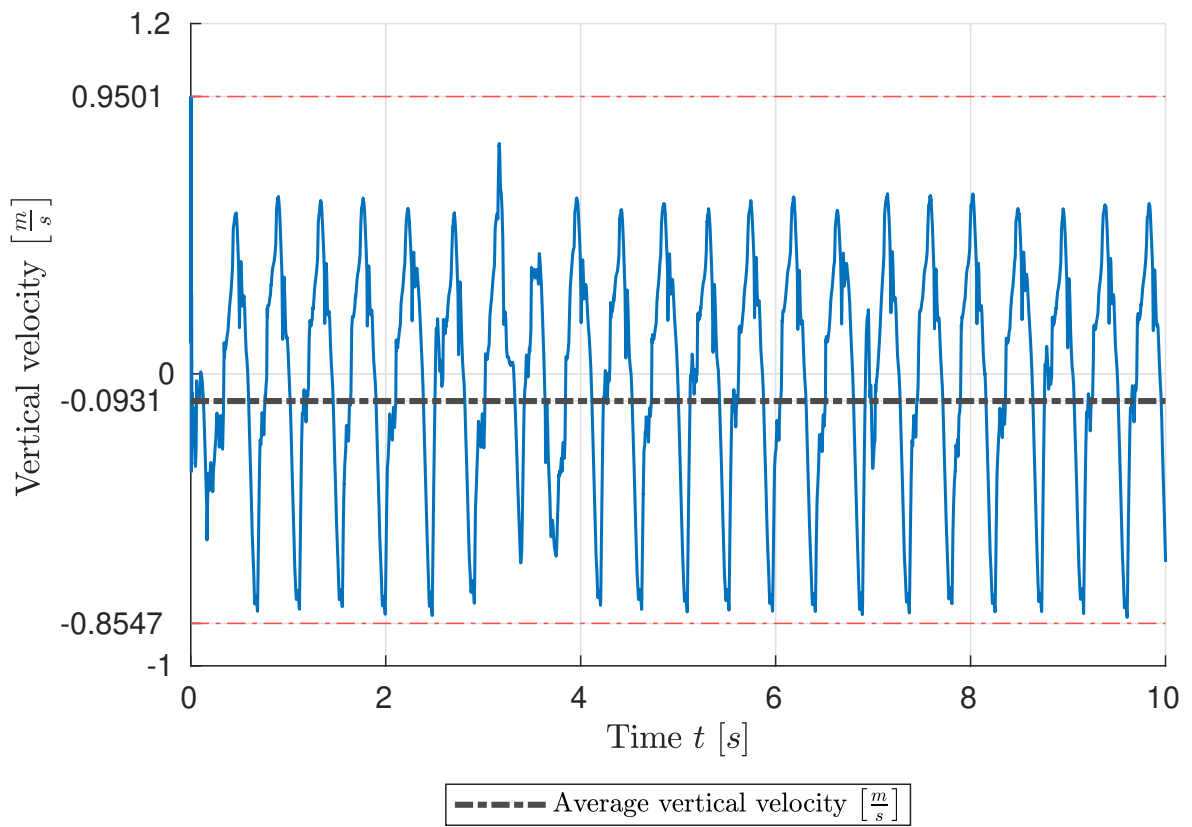


Figure B.1: The trajectory of the vertical velocity of the center of mass during the motion. For legibility purposes, the first 10 s of movement are displayed. The average vertical velocity is $-0.0931 \frac{m}{s}$. The amplitude of the vertical velocity ranges from a maximum of $0.9501 \frac{m}{s}$ to a minimum of $-0.8547 \frac{m}{s}$.

Bibliography

- [1] Alexander, R. M. “The Gaits of Bipedal and Quadrupedal Animals”. In: *The International Journal of Robotics Research* 3.2 (June 1984), pp. 49–59. DOI: 10.1177/027836498400300205.
- [2] Andrew Biewener, S. P. *Animal Locomotion*. Oxford University Press, Mar. 23, 2018. 256 pp. ISBN: 0191060852. URL: https://www.ebook.de/de/product/34926791/andrew_biewener_sheila_patek_animal_locomotion.html.
- [3] Baker, R. “The history of gait analysis before the advent of modern computers”. In: *Gait & Posture* 26.3 (Sept. 2007), pp. 331–342. DOI: 10.1016/j.gaitpost.2006.10.014.
- [4] Blickhan, R. “The spring-mass model for running and hopping”. In: *Journal of Biomechanics* 22.11-12 (Jan. 1989), pp. 1217–1227. DOI: 10.1016/0021-9290(89)90224-8.
- [5] Carrier, D. R., Kapoor, A. K., Kimura, T., Nickels, M. K., Scott, E. C., So, J. K., and Trinkaus, E. “The Energetic Paradox of Human Running and Hominid Evolution [and Comments and Reply]”. In: *Current Anthropology* 25.4 (Aug. 1984), pp. 483–495. DOI: 10.1086/203165.
- [6] Cavagna, G. A., Heglund, N. C., and Taylor, C. R. “Mechanical work in terrestrial locomotion: two basic mechanisms for minimizing energy expenditure”. In: *American Journal of Physiology-Regulatory, Integrative and Comparative Physiology* 233.5 (Nov. 1977), R243–R261. DOI: 10.1152/ajpregu.1977.233.5.r243.
- [7] Donelan, J. M., Kram, R., and Kuo, A. D. “Simultaneous Positive and Negative External Mechanical Work in Human Walking”. In: *Journal of Biomechanics* 35.1 (Jan. 2002), pp. 117–124. DOI: 10.1016/s0021-9290(01)00169-5.
- [8] Full, R. J. and Tu, M. S. “Mechanics of a rapid running insect: two-, four- and six-legged locomotion”. In: *Journal of Experimental Biology* 156.1 (Mar. 1991), pp. 215–231. DOI: 10.1242/jeb.156.1.215.
- [9] Gallagher, J. C., Beer, R. D., Espenschied, K. S., and Quinn, R. D. “Application of evolved locomotion controllers to a hexapod robot”. In: *Robotics and Autonomous Systems* 19.1 (Nov. 1996), pp. 95–103. DOI: 10.1016/s0921-8890(96)00036-x.
- [10] Geng, T., Porr, B., and Wörgötter, F. “Fast Biped Walking with a Sensor-driven Neuronal Controller and Real-time Online Learning”. In: *The International Journal of Robotics Research* 25.3 (Mar. 2006), pp. 243–259. DOI: 10.1177/0278364906063822.
- [11] Genin, J. J., Willems, P. A., Cavagna, G. A., Lair, R., and Heglund, N. C. “Biomechanics of locomotion in Asian elephants”. In: *Journal of Experimental Biology* 213.5 (Mar. 2010), pp. 694–706. DOI: 10.1242/jeb.035436.
- [12] Geyer, H., Seyfarth, A., and Blickhan, R. “Compliant leg behaviour explains basic dynamics of walking and running”. In: *Proceedings of the Royal Society B: Biological Sciences* 273.1603 (Aug. 2006), pp. 2861–2867. DOI: 10.1098/rspb.2006.3637.

- [13] Goswami, A., Espiau, B., and Keramane, A. "Limit cycles and their stability in a passive bipedal gait". In: *Proceedings of IEEE International Conference on Robotics and Automation*. IEEE. DOI: 10.1109/robot.1996.503785.
- [14] Griffin, T. M., Main, R. P., and Farley, C. T. "Biomechanics of quadrupedal walking: how do four-legged animals achieve inverted pendulum-like movements?" In: *Journal of Experimental Biology* 207.20 (Sept. 2004), pp. 3545–3558. DOI: 10.1242/jeb.01177.
- [15] Grillner, S. "Locomotion in vertebrates: central mechanisms and reflex interaction". In: *Physiological Reviews* 55.2 (Apr. 1975), pp. 247–304. DOI: 10.1152/physrev.1975.55.2.247.
- [16] Hildebrand, M. "Symmetrical Gaits of Horses". In: *Science* 150.3697 (Nov. 1965), pp. 701–708. DOI: 10.1126/science.150.3697.701.
- [17] Hildebrand, M. "Symmetrical gaits of dogs in relation to body build". In: *Journal of Morphology* 124.3 (Mar. 1968), pp. 353–359. DOI: 10.1002/jmor.1051240308.
- [18] Hubicki, C., Abate, A., Clary, P., Rezazadeh, S., Jones, M., Peekema, A., Why, J. V., Domres, R., Wu, A., Martin, W., Geyer, H., and Hurst, J. "Walking and Running with Passive Compliance: Lessons from Engineering: A Live Demonstration of the ATRIAS Biped". In: *IEEE Robotics and Automation Magazine* 25.3 (Sept. 2018), pp. 23–39. DOI: 10.1109/mra.2017.2783922.
- [19] Irschick, D. and Jayne, B. "Comparative three-dimensional kinematics of the hindlimb for high-speed bipedal and quadrupedal locomotion of lizards". In: *Journal of Experimental Biology* 202.9 (May 1999), pp. 1047–1065. DOI: 10.1242/jeb.202.9.1047.
- [20] Kajita, S. and Tani, K. "Study of dynamic biped locomotion on rugged terrain-derivation and application of the linear inverted pendulum mode". In: *Proceedings. 1991 IEEE International Conference on Robotics and Automation*. IEEE Comput. Soc. Press. DOI: 10.1109/robot.1991.131811.
- [21] Kelly, M. "An Introduction to Trajectory Optimization: How to Do Your Own Direct Collocation". In: *SIAM Review* 59.4 (Jan. 2017), pp. 849–904. DOI: 10.1137/16m1062569.
- [22] Kuo, A. D., Donelan, J. M., and Ruina, A. "Energetic Consequences of Walking Like an Inverted Pendulum: Step-to-Step Transitions". In: *Exercise and Sport Sciences Reviews* 33.2 (Apr. 2005), pp. 88–97. DOI: 10.1097/00003677-200504000-00006.
- [23] Lee, C. R. and Farley, C. T. "Determinants of the center of mass trajectory in human walking and running." In: *Journal of Experimental Biology* 201.21 (Nov. 1998), pp. 2935–2944. DOI: 10.1242/jeb.201.21.2935.
- [24] Lee, D. V., Bertram, J. E. A., Anttonen, J. T., Ros, I. G., Harris, S. L., and Biewener, A. A. "A collisional perspective on quadrupedal gait dynamics". In: *Journal of The Royal Society Interface* 8.63 (Apr. 2011), pp. 1480–1486. DOI: 10.1098/rsif.2011.0019.
- [25] Lee, D. V., Comanescu, T. N., Butcher, M. T., and Bertram, J. E. A. "A comparative collision-based analysis of human gait". In: *Proceedings of the Royal Society B: Biological Sciences* 280.1771 (Nov. 2013), p. 20131779. DOI: 10.1098/rspb.2013.1779.
- [26] Lee, D. V. and Harris, S. L. "Linking Gait Dynamics to Mechanical Cost of Legged Locomotion". In: *Frontiers in Robotics and AI* 5 (Oct. 2018). DOI: 10.3389/frobt.2018.00111.
- [27] Lipfert, S. W., Günther, M., Renjewski, D., Grimmer, S., and Seyfarth, A. "A model-experiment comparison of system dynamics for human walking and running". In: *Journal of Theoretical Biology* 292 (Jan. 2012), pp. 11–17. DOI: 10.1016/j.jtbi.2011.09.021.

- [28] MATLAB. *version 9.12.0.2170939 (R2022a) Update 6*. Natick, Massachusetts: The Math-Works Inc., 2022.
- [29] Maus, H.-M., Lipfert, S., Gross, M., Rummel, J., and Seyfarth, A. “Upright human gait did not provide a major mechanical challenge for our ancestors”. In: *Nature Communications* 1.1 (Sept. 2010). DOI: 10.1038/ncomms1073.
- [30] McMahon, T. A. and Cheng, G. C. “The mechanics of running: How does stiffness couple with speed?” In: *Journal of Biomechanics* 23 (Jan. 1990), pp. 65–78. DOI: 10.1016/0021-9290(90)90042-2.
- [31] Renjewski, D. “Robotic Spring-Mass Walkers - Potential and Limitations”. In: *Dynamic Walking*. 2012.
- [32] Renjewski, D. *An Engineering Contribution to Human Gait Biomechanics*. Verlag Dr. Kovac, 2013, p. 140. ISBN: 9783830068587.
- [33] Renjewski, D. *[Schematic representation of the JenaFox robot]*. [Applied Biorobotics (Module MW2388): Online; accessed January 22, 2023]. URL: <https://www.moodle.tum.de/course/view.php?id=75052>.
- [34] Renjewski, D. *[The extensor and flexor joint angles of the Jenafox robot]*. [Applied Biorobotics (Module MW2388): Online; accessed January 22, 2023]. URL: <https://www.moodle.tum.de/mod/page/view.php?id=2068770>.
- [35] Reynolds, T. R. “Stride length and its determinants in humans, early hominids, primates, and mammals”. In: *American Journal of Physical Anthropology* 72.1 (Jan. 1987), pp. 101–115. DOI: 10.1002/ajpa.1330720113.
- [36] Rummel, J., Blum, Y., Maus, H. M., Rode, C., and Seyfarth, A. “Stable and robust walking with compliant legs”. In: *2010 IEEE International Conference on Robotics and Automation*. IEEE, May 2010. DOI: 10.1109/robot.2010.5509500.
- [37] Siciliano, B. and Khatib, O., eds. *Springer Handbook of Robotics*. Springer International Publishing, 2016. DOI: 10.1007/978-3-319-32552-1.
- [38] Sitti, M., Menciassi, A., Ijspeert, A. J., Low, K. H., and Kim, S. “Survey and Introduction to the Focused Section on Bio-Inspired Mechatronics”. In: *IEEE/ASME Transactions on Mechatronics* 18.2 (Apr. 2013), pp. 409–418. DOI: 10.1109/tmech.2012.2233492.
- [39] Van Bommel, L. *Virtual pivot point control for running robots*. 2011. URL: <http://resolver.tudelft.nl/uuid:11f0f72d-bd6b-4577-a0e1-8befd6c68142>.
- [40] Vernon, D. *Artificial Cognitive Systems. A Primer*. MIT Press, 2014, p. 288. ISBN: 9780262028387.